Submitted to the Physical Review B

LBL-1688
Preprint

TOTAL VALENCE-BAND DENSITIES OF STATES OF III-V AND II-VI COMPOUNDS FROM XPS

L. Ley, R. A. Pollak, F. R. McFeely,
S. P. Kowalczyk, and D. A. Shirley

May 1973

Prepared for the U. S. Atomic Enegy Commission
under Contract W-7405-ENG-48

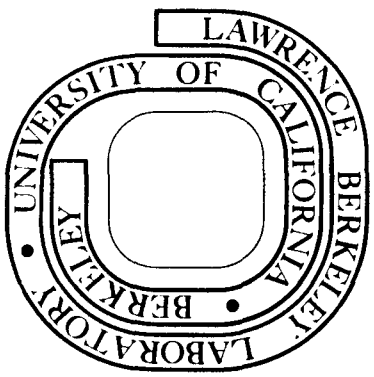

DISCLAIMER

TOTAL VALENCE-BAND DENSITIES OF STATES OF III-V AND II-VI COMPOUNDS FROM XPS*

L. Ley, R. A. Pollak†, F. R. McFeely, S. P. Kowalczyk, and D. A. Shirley

Department of Chemistry and
Lawrence Berkeley Laboratory
University of California
Berkeley, California 94720

May 1973

ABSTRACT

A comprehensive survey of the total valence-band XPS spectra of 14 semiconductors is reported. The x-ray photoelectron spectra of cubic GaP, GaAs, GaSb, InP, InAs, InSb, ZnS, ZnSe, ZnTe, CdTe, and HgTe, and of hexagonal ZnO, CdS, and CdSe were obtained from freshly-cleaved single crystals, in the 0 - 50 eV binding-energy range, using monochromatized Al Kα (1486.6 eV) radiation. The binding energies of the outermost d-shells are reported. They were determined relative both to the top of the valence bands (E_B^V) and to the Fermi level of a thin layer of gold that was vapor-deposited after each run (E_B^F). These data also yielded accurate measures of sample charging, which was found to be approximately equal to the band gap. A mechanism for this result is discussed. The Fermi level fell near the center of the gap for six samples, near the top for two, and near the bottom for three. Evidence for an apparent increase in core d-level spin-orbit splitting over free-atom values was interpreted as a possible spreading of a Γ_7 and a Γ_8 level from the upper ($d_{3/2}$) Γ_8 level by a tetrahedral crystal field.

The s,p valence-band spectra showed three main peaks, with considerable structure on the "least-bound" peak. A discussion is given of the validity of comparing the VB spectrum I'(E) with the VB density of states, including

cross-section modulation, final-state modulation, and relaxation effects. Characteristic binding energies of spectral features in I'(E) are tabulated. In addition, the energies of the characteristic symmetry points L_3, X_5, W_2, Σ_1^{min}, W_1, $X_3(L_1)$, X_1, L_1, and Γ_1 are given for the eleven cubic compounds. These are compared with UPS results where available and with theoretical band-structure results from the EPM, OPW, OPW(adj), SCOPW, APW, KKR, and ROPW, $X_{\alpha\beta}$ methods, where available. The ROPW, $X_{\alpha\beta}$ energies agree very well with experiment, on the whole. In particular, they predict the important "ionicity gap" $X_1 - X_3$ quite accurately. The EPM densities of states provided a useful basis for relating features in I'(E) to energies of the characteristic symmetry points. Band-structure calculations in combination with XPS spectra appear to provide a very powerful approach to establishing the total valence-band structure of semiconductors.

I. INTRODUCTION

The group IV and $A^{N}B^{8-N}$-type semiconductors have been extensively studied because of their technical and scientific importance. The electronic band structures of these materials are among their most fundamental properties. Optical measurements and band-structure calculations have played complementary and often interdependent roles in the elucidation of electronic band structures in these materials. A detailed interpretation of optical reflectance or ε_2 data is seldom possible without at least a semi-quantitative band structure calculation because the optical excitations fall in an energy range where both conduction and valence bands contribute significantly to the observed structure. The reliability of these calculations in turn depends on the correct interpretation of certain key features in the optical data. This process of determining band structure is clearly one of trial and error, but it often leads to a consistent, quantitative, detailed picture of the band structure of semiconductors in a limited range of energy around the fundamental gap. Nevertheless, this point has not yet been reached for a great number of semiconductors, although excellent and detailed optical data are in many cases available. Clearly, reliable initial and final-state energies are needed. Progress in assigning initial and final-state energies to optical transitions has been made by using data from UV photoemission spectroscopy (UPS). The UPS data are closely related to those of optical spectroscopy. Information obtained from UPS spectra in which the energy of the exciting radiation is varied allows in conjunction with detailed band structure calculations separate determinations of the energies of initial and final states for direct transitions. The UPS work of Shay and Spicer[1] on CdTe, for instance, led to a reinterpretation of the reflectivity data of Cardona and Greenaway,[2] because Shay and Spicer were able to assign absolute binding energies to several critical points in the band structure.

At UPS energies valence-band and conduction band electronic structure and $\vec{k}$ conservation dictate the electronic transition probability. As the energy of the exciting radiation increases, the density of final states is expected to become relatively flat and unstructured and the $\vec{k}$ selection rule is readily fulfilled without introducing additional structure. As a qualitative rule-of-thumb, this behavior is expected when the transition energy far exceeds variations in the crystal potential energy of the valence electrons. Thus for $h\nu \gtrsim 50 - 100$ eV, the final-state density should be fairly constant.[3] Although the photoemission spectrum may still not resemble the valence-band density-of-states, because of cross-section modulation, this modulation alone is found to be less severe than that due to final-state structure at low photon energies.[4] It is therefore possible to deduce from high-energy photoemission spectra the valence density-of-states with less ambiguity than from either low energy UPS or optical measurements.

In this paper we report the x-ray induced photoemission spectra of fourteen binary semiconductors, obtained with monochromatized Al $K\alpha_{1,2}$ radiation (1486.6 eV). A comparison of calculated densities of states for several of these compounds with our spectra forms the basis for the determination of the binding energies corresponding to a selected set of critical points in the valence bands. These valence-band energies are compared in Sec. IV with available theoretical results. In Sec. II we describe experimental procedures, and in Sec. III the spectra of the outermost d-levels and the position of the Fermi level are discussed.

II. EXPERIMENTAL

A. Apparatus

Until recently experimental limitations have restricted x-ray photoemission valence band studies to systems with valence bands composed largely of d-electron bands or else to systems with s- and p-bands but with no d-levels nearby. These limitations resulted from poor signal-to-background ratios caused both by bremsstrahlung radiation and also by $K\alpha_{3,4}$, etc., x-rays which are present when conventional unfiltered x-ray sources are employed. The problems are exacerbated by the fact that x-ray photoelectric cross sections for s- and p-electrons are smaller than for d-electrons in the valence band region.

The measurements reported here were obtained with a Hewlett-Packard HP 5950A ESCA photoelectron spectrometer[5] which uses monochromatized Al $K\alpha_{1,2}$ x-rays (1486.6 eV). Monochromatization removes the bremsstrahlung background radiation and satellite x-rays, thereby greatly reducing the background, enhancing the signal-to-background ratio, and allowing the observation of weak s- and p-band peaks even in the presence of strong d-peaks.

The instrumental resolution has been obtained from the slope of the Fermi edges in the spectra of Pd, Ag, Cd, In, and Sn.[6] For each of these cases the observed slope can be obtained by folding a Fermi distribution function with a Gaussian instrumental response function of 0.55 ± 0.02 eV FWHM. The error applies only to the precision of the measurement.

During the experiments reported here the residual gas pressure in the HP 5950A analyzer chamber ranged from 5×10^{-9} Torr to 3×10^{-8} Torr. The total pressure was measured with a nude Bayard-Alpert gauge and the partial pressures with a quadrupole mass spectrometer. The residual gas in the unbaked system

consists mainly of water, CO, and H_2, with small quantities of hydrocarbons and rare gases. X-ray photoemission samples a relatively thick "surface" layer of material in contrast to high-energy UV photoemission. Thus even in the vacuum of the unbaked system we believe that the spectra were not significantly affected by surface impurities.

B. Sample Preparation

All samples were single crystals. Their structure and quality were checked by x-ray powder diffraction. Structural data are given in Table I.

To produce a clean surface each sample was cleaved in an inert atmosphere just prior to insertion into the vacuum chamber. A glove bag was placed over the insertion port of the spectrometer and repeatedly flushed with dry N_2 evaporated from liquid nitrogen. The sample was cleaved, then introduced directly into the vacuum of the spectrometer. This method reduced surface contaminants to levels at which they did not noticeably affect the valence-band structure, as shown by suitable control experiments. A measure of the carbon and oxygen present is given in Table II. The oxygen contamination is given in fractions of monolayers of adsorbed atoms as estimated from a comparison of the contaminant oxygen 1s peak with the same peak in ZnO. The active sample depth for ZnO was assumed to be $\sim$ 20 Å. Even for the samples with the highest oxygen contamination (Table II), no lines in the photoemission spectrum could be detected which correspond to the formation of an oxide of either of the components of the binary compounds.

C. The Reference Energy and Charging

In x-ray photoemission from solids the energies of characteristic spectral features are measured directly relative to the Fermi energy of the

spectrometer; i.e., the energy actually measured is the kinetic energy of the electrons within the analyzer. For a metallic sample that is securely grounded to the spectrometer, the binding energy E_B^F of a given spectral feature relative to the Fermi level is given in terms of its kinetic energy K by

$$E_B^F = h\nu - K - e\phi_{sp} \quad , \tag{1}$$

where $h\nu$ is the initial photon energy and $e\phi_{sp}$ (a positive quantity) is the electron charge times the spectrometer work function. Alternatively the Fermi energy may be identified directly as a Fermi edge in the photoelectron spectrum and the binding energy E_B^F of a given spectral feature may be obtained by direct comparison. While E_B^F is of interest, it is often desirable to know E_B^V, the binding energy with respect to the vacuum level. The two are related for a metal by

$$E_B^V = E_B^F + e\phi_s \quad , \tag{2}$$

where ϕ_s is the sample's work function. Since x-ray photoemission is not sensitive to ϕ_s, this quantity must be obtained from other measurements.

In semiconductors and insulators the situation is more complicated. The sample may become charged, thereby shifting its effective Fermi energy relative to that of the spectrometer. Then E_B^F can be determined neither directly, by an absolute measurement of electron kinetic energy, nor by comparison to a Fermi edge, as there is none. It is possible to establish the position of a Fermi level, and we have done so, as described below, but its meaning is dubious. Thus we also quote binding energies E_B^V relative to E_{VB}, the energy of the top of the valence bands, which we prefer as a reference energy.

In x-ray photoemission, x-rays striking the sample produce photoelectrons, and these in turn can excite secondary electrons. Many of these electrons are sufficiently energetic to leave the sample at the surface from which photoelectrons are being analyzed. This surface becomes positively charged until the photoelectron-plus-secondary current I_e is counterbalanced by a neutralizing current I_n originating from ground or from ambient space charge. The currents I_e and I_n depend on many properties of the sample, on the way in which the sample is mounted, and on the spectrometer. When the steady state corresponding to $I_e = I_n$ is established, a Volta potential ψ will be established. The sample will be positively charged and the whole spectrum shifted to lower kinetic energies, with the apparent binding energies now given by

$$E_B^{App} = h\nu - K - e\phi_{sp} + e\psi \quad . \tag{3}$$

Of course E_B^{App} is the apparent binding energy of electrons that are observed; i.e. those emitted from atoms in the effective part of the sample. Since the scattering length of $\sim$ 1 keV electrons in solids is typically $\sim$ 20 Å, the effective sample is no more than $\sim$ 20 - 100 Å deep, i.e., nearly all the electrons that leave the sample with zero energy loss, to be analyzed in the "full energy" photoelectron peaks, originate within 100 Å of the surface. Since the entire Volta potential ψ arises over a sample thickness corresponding to x-ray penetration depths, or 10^4 - 10^5 Å, it is reasonable to expect the voltage drop across the surface 10^2 Å or so, which would show up as line broadening, to amount to a very small fraction of ψ. This must in fact be the case for the samples studied in this work, because sharp lines were observed even in the presence of Volta potentials of 10 volts or more.

The above arguments would be consistent with sharp lines in the absence of lateral potential gradients across the sample surface. Our samples were single crystals, and it seems quite probable that high surface conductivity under the conditions of x-ray irradiation in the spectrometer insured that the entire effective sample (a region with dimensions 1 mm × 5 mm × 100 Å) was at the same potential. Clearly this condition would be more difficult to achieve in a polycrystalline sample.

In the Hewlett-Packard 5950A spectrometer the sample is irradiated by a focused x-ray beam. Thus an area 1 mm × 5 mm in the center of the ∿ 1 cm × 1 cm sample is exposed to x-rays and maintained at a constant potential, while the perimeter, which is not irradiated, provides a resistive path to ground that can support Volta potentials of up to 10 volts or more in some cases. In this work the Volta potentials were determined as follows. After each sample had been studied thoroughly, a thin layer of gold was evaporated onto the sample in situ. The energy of the gold $4f_{7/2}$ line was recorded together with that of a strong core-level peak from the substrate (i.e., the sample). Since the gold $4f_{7/2}$ line is known to lie at $E_B^F = 84.00 \pm 0.01$ eV in gold,[7] the substrate core-level peak was thereby referenced to the Fermi level of the gold film. Referring back to the position of the core-level peak before the gold film was added, we could then derive both the position of the Fermi energy E_F relative to the valence bands and the apparent position of E_F on an absolute scale (hence ψ). Although this approach gave consistent and sensible results, we cannot be completely confident that the gold evaporation did not alter the sample in some way (e.g., by moving E_F relative to the valence bands). Figure 1 shows the Volta potential measured in this way, plotted against the band gap for 26 semiconductors and insulators.

The general trend in Fig. 1 is for charging to increase with band gap. The materials with small band gaps charge to values near or less than the band gap, and those with large band gaps charge to values near or greater than the band gap. The unusually high charging in ZnSe (22 eV) is probably attributable to the photovoltaic effect. Exceptionally high photovoltages have been reported for ZnSe single crystals.[8]

The fact that charging follows the band gap so closely suggests that a mechanism such as Zener breakdown switches on a higher I_n at Volta potentials near the band gap value. This mechanism is especially likely in the materials with thin depletion layers (high carrier concentrations). The depletion layer in this case is the region between the irradiated and non-irradiated portion of the sample. As the depletion layer gets thicker (carrier concentration decreases) one expects the charging to increase above the band gap value. We see this behavior in the alkali halides (Fig. 1). Breakdown by carrier multiplication (avalanche breakdown) would tend to limit this increased charging effect. Surface conductivity must also be considered. It may contribute significantly to I_n in those cases in which the charging is less than the band gap. Bulk conductivity in small band gap materials can also limit the charging to values less than the band gap. Finally the possibility of non-ohmic contact between sample and spectrometer adds another degree of complexity to the charging problem and should be avoided. When the data in Fig. 1 were taken we did not anticipate that the Volta potential might be related to the band gap as closely as Fig. 1 suggests, and we did not therefore take special precautions to assure ohmic contact to ground. Perhaps samples prepared with more attention paid to this aspect of the problem would yield closer agreement between the Volta potential and the band gap.

The above procedures yield at best the position of a Fermi energy E_F relative to the valence bands, but the meaning of this E_F is rather unclear. Even in a semiconductor "at rest" the position of the Fermi energy is strongly dependent on the nature and concentration of impurities. Under the conditions of these experiments (strong x-ray and photoelectron fluxes), the Fermi level is even less meaningful. This statement also applies to the various methods that one might devise to null out the Volta potential, such as irradiation with low-energy electrons or ultraviolet radiation, to establish a conducting path to ground. Of course either of these approaches would have the effect of setting the entire effective sample at the same potential.

The energy E_{VB} of the top of the valence bands provides a more useful reference for binding energies. The use of monochromatized x-rays greatly facilitates the determination of E_{VB}, which was accomplished in this work by extrapolating the steep leading edge of the highest valence-band peak to the baseline.

Table III lists the difference $E_{VB} - E_F$ for 11 semiconductors (the sign convention is that $E_{VB} - E_F$ is positive if E_F is in the gap), together with the gap energies. Since we have little confidence about the meaning of E_F as measured in the way described above, we do not wish to interpret $E_{VB} - E_F$ in any detail, but the observed trend of this difference will be compared with results of other workers in the next section.

III. CORE LEVELS AND THE FERMI ENERGY

The uncorrected photoelectron energy distributions for the binding energy range -4 to 45 eV are given in Figs. 2-6. The accumulation time for these spectra was typically 6 to 10 hours. The most intense features are the d-level peaks of the cations centered around 15 eV binding energy and those of the anions, around 35 eV. The Hg $5d_{3/2}$ - $5d_{5/2}$ doublet is well resolved, as are the spin-orbit split d-levels of Sb and Te. Additional structure typically 5% to 10% as intense as the d-level peaks is observed in the E_B^V = 0 - 15 eV region. This structure is attributed in each case to the valence bands formed from the outermost atomic s- and p-orbitals of the two constituent elements. Broad, asymmetric peaks, comparable in intensity to the valence electron distributions, are observed at kinetic energies about 10 eV below the d-levels. This structure results from photoelectrons excited from the d-levels which subsequently suffer inelastic energy losses. Most of this structure can be attributed to plasmon excitations and will be discussed elsewhere.[9] Similar inelastic loss structure is observed for all core levels.

A. The d-Levels

The binding energies obtained for the outermost cationic and anionic d-levels of the semiconductors are set out in Tables IV and V, respectively. The values are given both with respect to the Fermi level E_B^F using gold as a reference as outlined in Sec. II and also with respect to the top of the valence band E_B^V. This allows comparisons both with earlier photoemission work which used a metal or carbon surface layer as a reference and also with UPS experiments, in which energies are referred to the top of the valence band.

The binding energy for each spin-orbit split component is given for resolved doublets. In ZnSe and PbSe a weighted mean value is also given, to facilitate comparison with unresolved data. The weighting factors used were the multiplicities of the states. The fourth columns of Tables IV and V list the experimental method and the reference element (carbon or gold) used for each reported set of binding energies.

The errors quoted for the binding energies E_B^F are usually smaller than those for E_B^V, because the determination of the reference peak position (Au $4f_{7/2}$ in the present work) is more accurate than the determination of the top of the valence band. Of course the errors in E_B^V represent accuracy since E_{VB} is a well-defined quantity, while those in E_B^F represent only precision.

The agreement between our data and the binding energies E_B^F from earlier XPS work[10-13] is generally very good. No systematic deviations of binding energies obtained by different groups or with different methods of referencing (Au or C) were observed.

Turning now to E_B^V, the binding energies with respect to the top of the valence bands, we can compare our data for the d-levels of the cations in most of these compounds with the UPS results.[1,14-18] The binding energies measured by Veseley, Hengehold, and Langer[15] for the Cd 4d levels and the Zn 3d level in ZnO are consistently higher than those of Shay and Spicer[1,14] and of Powell, Spicer, and McMenamin[16] by approximately 0.8 eV except for CdTe, where the difference is only 0.2 eV. Our results favor the results of Shay and

Spicer,[1,14] for CdSe and those of Veseley et al.[15] for ZnO. For CdTe and ZnSe all binding energies agree quite well while in ZnTe the UPS binding energies of Veseley et al.[15] are 0.7 eV low. Additional measurements are needed to substantiate apparent deviations and resolve remaining ambiguities in these binding energies. For most of the more tightly bound core levels ($E_B^V \gtrsim 15$ eV) we report the first binding energies with respect to the top of the valence band, since these energies are not accessible to conventional UV work.

Our contributions to this compilation lie in the improved accuracy of the binding energies of outer d-levels of semiconducting compounds and in the unique possibility of comparing different referencing methods with the same sample under identical experimental conditions. In the discussion of our results we will emphasize these two aspects and refer the reader to the papers of Veseley et al.[12,15] for a comparison of experimental and theoretical core-level binding energies.

B. Position of the Fermi Level Within the Fundamental Gap

The position of the Fermi level as measured in photoemission experiments depends upon stoichiometry, doping, and surface states. Band bending resulting from charging of the surface must also be considered. It has been shown that in order to understand the position of the Fermi level within the gap, great care must be taken to control each of the aforementioned parameters.[19] Experiments must be done on samples with atomically clean surfaces and one must know the stoichiometry and doping, which are less controllable in the binary semiconductors than in, for example, Si and Ge. Most photoemission experiments to date have been done on samples for which at least one and more often more of the above parameters were not well defined. A few ultra-high vacuum ultraviolet

photoemission experiments are exceptions.[19,20] All x-ray photoemission experiments reported to date including those reported here have been done under conditions where the parameters necessary to determine and explain the position of the true Fermi level within the gap are not well-defined. We have modified our spectrometer to operate with ultra-high vacuum and we plan to study this problem under more well-defined conditions. For the present results we shall simply make the following empirical observations.

As described in Sec. II C we used a thin layer of gold applied to the semiconductor surface to obtain an experimentally determined reference point which we call the gold-referenced Fermi level E_F. In Table III we report the position of E_F within the fundamental gap for 11 semiconductors. This table lists for each material the position of E_F above the top of the valence bands and the measured band gaps obtained from the literature. We have also indicated whether E_F falls closest to the top (T), center (C), or bottom (B) of the fundamental gap, where the bottom of the gap coincides with the top of the valence band. The results show that E_F is preferentially pinned neither to the top of the gap as suggested by Gudat et al.[10] nor do we find it considerably in the center of the gap as was the case in the investigation of Veseley, Hengehold, and Langer.[15] The latter authors determined the position of E_F for CdS, CdSe, CdTe, ZnO, ZnSe, ZnTe and in addition for the small gap semiconductors HgSe and HgTe by comparing E_B^V from UV-measurements with E_B^F from XPS data (see Table IV). Differences in E_B^V (see Sec. III A) explain the disagreement between our results and theirs for the position of E_F in CdSe and ZnTe.

C. Spin-Orbit Splitting in the Outer d Shells

Binding-energy differences in the spin-orbit split outer d-shells of these elements provides a sensitive test of the effect of crystal fields on the apparent spin-orbit splitting in closed shells. We note that p-shells would not be affected by cubic crystal fields, while tightly-bound core levels would be less affected by the crystalline environment than would the outer d levels.

In the $4d5s5p$ elements Pollak et al.[6] observed anomalously large apparent spin-orbit splitting of the $4d_{3/2}$ and $4d_{5/2}$ subshells of Cd and possibly In. These results were attributed to the combined effect of spin-orbit interaction and crystal-field interaction. While crystal-field forces would mix the $d_{3/2}$ and $d_{5/2}$ levels and alter the spectrum from the characteristic multiplet pattern, these effects could appear as an increase in the splitting of an unresolved doublet for small values of the crystal field. Later work by Poole, et al.[21] has confirmed these results and extended them to Zn, while Cardona, et al.[18] have called attention to the systematically smaller splittings observed in InSb and PbTe than in elemental In, Sb, and Te. The data obtained in the present work adds sufficiently to the total available on this effect that a brief general discussion of the present experimental situation seems warranted.

Spin-orbit coupling is described by the Hamiltonian

$$\mathcal{H}_{s-o} = \frac{\alpha^2}{2} \left(\frac{1}{r} \frac{\partial V}{\partial r}\right) \vec{L} \cdot \vec{S}$$

where α is the fine-structure constant and V is the electrostatic potential and $\vec{L}$ and $\vec{S}$ are the orbital and spin angular momentum operators, respectively. Apparent variations in the effective $d_{3/2} - d_{5/2}$ splitting in a crystal lattice

could arise either from actual variations in $\mathcal{H}_{s-o}$ or from additional interactions. Only the first alternative would be a true change in the spin-orbit interaction. It would involve an alteration of the (monopole-symmetry) term $\frac{1}{r}\frac{\partial V}{\partial r}$. If such an effect were important it would show up as an increase in the spin-orbit splitting from free cations to ionic solids and as a corresponding decrease for anions. No such regular variation is in fact observed. Rough estimates based on point-charge models indicate that expected variations in $\frac{1}{r}\frac{\partial V}{\partial r}$ in ionic solids would alter the spin-orbit splitting by 10^{-3} eV or less. Finally, comparisons of ΔE_{s-o} in different charge states of free ions shows only a very slight dependence on charge state. The atomic data[22] for these elements are listed in Table VI, along with ΔE_{s-o} results from this work and other photoemission results on solids.[6,12,17,18,21,23,24] Since ionization of a valence electron would affect $\frac{1}{r}\frac{\partial V}{\partial r}$ far more than would a change in the ionic environment, this result, together with the above two, leads us to conclude that changes in $\mathcal{H}_{s-o}$ are not responsible for apparent changes of ΔE_{s-o} in these solids. Variations in the apparent splitting must therefore result from crystal field interactions of higher than monopole symmetry.

We note first that the simple elements showing increases in ΔE_{s-o} from gas to solid all have lower than cubic symmetry. These will be discussed separately elsewhere.[25] The III-V and II-VI semiconductors of interest here all have tetrahedral point symmetry about a lattice site, in the wurtzite and zincblende structures. Under the combined interaction of spin-orbit coupling and an octahedral crystal field, the energy levels of a single d-electron are resolved into one Γ_7 level at

$$E(\Gamma_7) = -4Dq + \xi \quad ,$$

with twofold total degeneracy including spin degeneracy, and two Γ_8 levels at

$$E_1(\Gamma_8) = 6Dq + \sqrt{\frac{3}{2}}\,\xi \cot\theta \quad ,$$

$$E_2(\Gamma_8) = -4Dq - \frac{1}{2}\,\xi - \sqrt{\frac{3}{2}}\,\xi \cot\theta \quad .$$

Each of the Γ_8 levels has a total degeneracy of four. Here ξ is the spin-orbit coupling constant and θ is defined by

$$\tan 2\theta = \frac{-\sqrt{6}\,\xi}{10Dq + \frac{1}{2}\,\xi} \quad .$$

These results were quoted by Ballhausen.[26] We can use them with only trivial changes to treat the problem of a single d-hole (the final state in a photoemission experiment) in a tetrahedral field. Since the tetrahedral field, like the octahedral field, resolves the d-levels into t_{2g} and e_g representations but in inverted order, we can simply replace -10Dq by an empirical splitting parameter B, and absorb all constant factors into B. We note that B may *a priori* have either sign in the III-V and II-VI compounds. The spin-orbit coupling constant ξ is of course negative for the hole state.

Figure 7 shows the variation of ΔE with B, for a single d-hole in a tetrahedral field. The units are the magnitude of the spin-orbit splitting at B = 0, namely $\frac{5}{2}\,|\xi|$, and ξ is taken as negative and held constant while B is varied. For B < 0, the apparent splitting between the upper Γ_8 level and the lower $\Gamma_7 - \Gamma_8$ doublet could increase significantly over $\frac{5}{2}\,|\xi|$ without the overall appearance of the spectrum being greatly altered, provided that the natural width of the component lines is fairly large, as would be the case for the

semiconductors discussed here. As the individual lines grow narrower, the effects of B should be detectable first as a broadening, and decrease in the peak height from the multiplet ratio, of the "$d_{5/2}$" line. In fact there is considerable evidence for this in these results. Finally, for component linewidths much narrower than separation energies, three resolvable peaks should appear.

Turning to the data in Table VI, it seems quite clear that the Te $4d_{3/2}$ - $4d_{5/2}$ separation is greater in the four tellurides than in ionic TeVII. Since the splitting in TeVII is itself probably enhanced by the high charge state, the evidence for crystal-field enhancement is quite strong. Referring to Fig. 7, enhancement of ΔE by $\sim$ 3% to 1.45 eV would correspond to a value of

$$|B/\xi| \sim 0.5 \quad ,$$

with the sign of B undetermined, for the tellurides. We must be cautious about accepting this as proof that crystal-field enhancement has actually been observed, however, because both Pb and Hg appear to show a decrease in ΔE in the compounds relative to the free atoms, which is impossible according to Fig. 7.

IV. THE VALENCE BANDS

The similarity of gross features in the valence-band spectra of the binary tetrahedrally coordinated semiconductors makes identification of the observed peaks straightforward. The valence-band spectrum consists in each case of three peaks originating from the outermost cation and anion s- and p-electrons. A cation d-level peak is also present in each case between 10 and 20 eV binding energy. All peaks in the indium and gallium compounds are well resolved with the In 4d and Ga 3d level below all valence bands, but the Cd 4d level masks the lowest valence band in the cadmium compounds, and the lowest valence band in the zinc compounds lies below the Zn 3d level. The spin-orbit split Hg 5d level masks the lowest valence band in HgTe.

A background correction was performed in two steps. First the d-peaks were subtracted from the spectra. Second, the contribution from inelastically-scattered electrons was subtracted. The shape of the inelastic tail of the valence bands in each case was assumed to be the same as that of the nearby d-level's inelastic tail. The uncertainty introduced by the first step in the correction affects the determination of the position of the lowest valence bands to a minor extent; this has been included in the errors quoted.

The uncorrected valence band spectra I(E) are shown in Figs. 2 to 6 and the corrected spectra I'(E) are displayed in Figs. 8-13. The overall similarity of these spectra makes it easy to extract a number of common features. We shall do so first in a completely empirical way, without any reference to band-structure calculations. Let us consider the generalized spectrum shown in Fig. 14. The valence band structure is grouped into three peaks, which we label PI, PII, and PIII in order of increasing binding energy. PII and PIII are separated by a gap of low or zero electron density which widens in proceeding

from III-V to II-VI compounds. The width of this gap may be determined by linear extrapolation of the steep edges of the respective peaks to the baseline, yielding energies EII and EIII. In some cases peak I is well-enough resolved from peak II to permit similar determination of EI, on the high binding-energy side of PI. The energies of the bottom and top of the valence bands are determined by linear extrapolations of the leading and trailing edges of peaks PI and PIII respectively. The top of the valence bands, so determined, is taken as the zero of energy and the bottom is labeled B. Peak PI, the broadest of the three valence-band peaks, exhibits resolvable fine structure in some cases. This is labeled I_1 and I_2. A shoulder labeled Sl on the high binding-energy side of peak PI is resolved in almost all cases. In some cases peak I_1 can be resolved into two components, labeled I_1 and I_1'. The binding energies of these features are listed in Table VII. Also included are the energies at which the peaks reach half their heights, labeled H_{IT} (top of peak I), etc.

Our results are compared in Table VIII with the UPS results of Eastman, Grobman, Freeouf, and Erbudak,[17] who used 20 to 90 eV synchrotron radiation to study five of these compounds. Because they also gave results for Ge, these are included in Table VIII, along with our values for Ge, reported earlier.[27] The general appearance of the UPS spectra is quite similar to that of the XPS measurements. They differ mainly in that the UPS curves show steeper leading edges on peak I and poorer definition of peak III. In other respects they are of roughly equal quality, with UPS showing better resolution but a poorer signal to background ratio. The position of the peak PII with respect to the top of the valence band is extremely well reproduced by both methods (the absolute average deviation is only 0.16 eV), making PII a reference point of high reliability, as is the top of the valence bands.

Toward higher binding energies the agreement is less satisfying: the absolute average deviations are 0.2 eV for PIII and 0.7 eV for the bottom of the valence bands. This disagreement probably results largely from the uncertainty in correcting for the large contribution of inelastically scattered electrons in this region of the lower energy UPS spectra. The binding energies for I_1 obtained from XPS data are an average of 0.45 eV higher than those obtained by UPS. The reasons for this systematic deviation may be the slightly better resolution of UPS or matrix element effects which emphasize parts of PI close to the top of the valence band more in UPS than in XPS. We note that the former reason alone would not account for the good agreement on the positions of PII.

Above we have compared XPS and UPS results, finding good, but not perfect, agreement. Before interpreting our results to yield energies of bands at symmetry points in the Brillouin zone, let us inquire more closely into what XPS and UPS spectra really measure and how they relate to the valence-band density of states. We shall discuss three main points: final state modulation, cross-section modulation, and relaxation. The first two pertain to the photoelectron and the third to the passive electrons. In ultraviolet photoemission spectroscopy it is well-known that the observed spectrum is modulated both by the one-electron initial state density and by the one-electron final state density in the conduction band, these being regarded as the state-density weighting factors appropriate to the "active" (photo-) electron. At this level of approximation it is clear that increasing the photon energy into the x-ray region will effectively eliminate final-state modulation, because the state density at 1480 eV should be essentially independent of the crystal potential. In fact it has been predicted[28] that increasing the photon

energies in UPS to > 20 eV would bring the UPS and XPS valence-band spectrum into agreement. Table VIII provides strong confirmation of this prediction for these semiconductors.

Cross-section modulation can be discussed in two parts. First, electrons in valence s-, p-, d-, and f-bands will in general have different cross-sections for photoemission, and the cross-section ratios (e.g., $\sigma(s)/\sigma(p)$) can also vary with photon energy. These variations have been discussed by Price[29] and by Gelius[30] for gases and more recently by Cavell, et al.[4] for solids. It is immediately clear from this that the XPS and UPS spectra $I'(E)$ and the one electron density of states $\rho(E)$ can all show different intensity variations with energy. There is, however, also a subtler but very important difference between XPS and UPS that should be emphasized as UPS photon energies are being increased into the 50 - 100 eV range: UPS is more sensitive to the wavefunction in the outer portion of the atomic cell, while XPS senses the wavefunction near the nucleus. The effect, which was discussed by Price[29] for molecules, is illustrated for carbon 2s and 2p states in Fig. 15. Since the photoemission transition matrix element has the form $\langle \psi | \vec{r} | x \rangle$, where ψ and x are respectively the initial valence-band state and the final continuum state of the photoelectron, it is clear that the major contribution to the cross section must come from that region of the atomic cell in which the curvature of ψ most nearly matches that corresponding to the de Broglie wavelength of the continuum final state. Thus UPS spectra detect mainly the outer (bonding) regions of the wavefunction, and are sensitive to variations of the radial wavefunction between the bottom and top of the band. The XPS spectra are relatively insensitive to this variation, particularly if the corresponding atomic function has radial nodes.

The third point--relaxation in the final state--is often completely ignored in valence-band photoemission spectroscopy, although early attention was called to the effect.[31] We note first that most band-structure calculations do not treat exchange self-consistently. Thus a "Koopmans' correction"[32] must be made before it is correct to use Koopmans' Theorem[33] in estimating binding energies. This is not, however, the only objection to comparing $I'(E)$ and $\rho(E)$ directly. Particularly for the deeper valence bands, which are beginning to take on corelike characteristics, final-state relaxation will tend to move the valence-band features such as PIII "up" toward the "top" of the valence bands relative to a $\rho(E)$ calculated self-consistently. This statement is of course independent of the method of measurement. We shall make no correction for this effect in the discussion below. Thus when we discuss energies of symmetry points in the Brillouin zone relative to the top of the valence bands, we are in reality referring to the energies of these symmetry points in the one-hole final-states spectrum, relative to the bottom of the hole-state valence band spectrum.

Despite these caveats it seems possible to obtain reasonable estimates of the energies of symmetry points. This is done below.

The great expenditures in calculating the band structure throughout an irreducible part of the Brillouin zone has limited the available theoretical densities of states to relatively few compounds. Therefore, in order to compare our experimental data with as wide a range of calculations as possible, it was necessary to derive from $I'(E)$ the energies of selected symmetry points. The theoretical densities of states $\rho(E)$ for 5 cubic binary compounds as calculated by the empirical pseudopotential method (EPM)[35] have been broadened with a gaussian of 0.7 eV FWHM at the top and 0.8 eV FWHM at the bottom of the valence band, to account for finite instrumental resolution plus lifetime broadening

which increases with increasing binding energy. Figure 16 shows as an example the close resemblance of this broadened density of states $\rho'(E)$ with the experimental spectrum $I'(E)$ for GaP. The positions of characteristic features in the theoretical density of states $\rho(E)$ which are associated with the energies E_i of critical points can be related to corresponding features in the broadened density of states $\rho'(E)$. Applying the same criteria which determine E_i in $\rho'(E)$ to $I'(E)$ yields in turn experimental values for E_i. The similarity in the band structure of all the cubic binary semiconductors allows an extension of this procedure to spectra for which no theoretical densities of states are yet available.

The eight valence electrons per unit cell in the zincblende structure occupy 4 bands which constitute the valence-band density of states. The point of triple degeneracy of bands 1, 2, and 3 (counted from the top of the valence band), Γ_{15}, marks the top of the valence band, and corresponds to the zero of energy in Tables VII through XIX. Next, $\rho(E)$ rises within about 1 eV to a flat, sloped top between points L_3 and X_5. This flat top is somewhat rounded in $\rho'(E)$, but the peak at X_5 is well-resolved in most spectra. The degeneracy of bands 1 and 2 is lifted along the symmetry line Σ between X_5 and Γ_{15}, and the lowest point Σ_1^{min} of band 2 marks the bottom of peak PI. In $\rho'(E)$ and $I'(E)$ Σ_1^{min} falls about halfway between the botton of peak PI and the shoulder which arises from a small sharp peak associated with the band at W_2. The near degeneracy of the symmetry points of band 3 over the surface of the Brillouin zone gives rise to the sharp peak PII. The top of this peak, which coincides within two tenths of an eV with W_1 is the feature which can most reliably be determined from $I'(E)$. The point X_3 usually marks the bottom of peak PII in $\rho(E)$.

Band 4 forms peak PIII, which is a distorted mirror image of peak PII. Points X_1 and W_4 on the square face of the Brillouin zone are again almost degenerate. They determine the spike and sharp leading edge (in $\rho(E)$) of peak PIII. The otherwise rather flat top breaks at L_1 into a smooth decrease in $\rho(E)$ toward the bottom of the valence band at Γ_1. After broadening, this richly structured band appears as a slightly asymmetric peak whose top marks fairly accurately the position of L_1. The positions of X_1 and W_4 fall at about three quarters of the height of peak PIII.

Applying the criteria which determine the position of the symmetry points in $\rho'(E)$ to $I'(E)$ of the cubic compounds we obtain the binding energies of these points with respect to the top of the valence band at Γ_{15}. These results are listed and compared with pertinent calculations[35-44] in Tables IX-XIX. The results from UPS measurements[17] are also given for comparison, where available.

Among the band-structure calculations we can distinguish two classes: first-principles calculations such as OPW and KKR (Green's function method) which start with a muffin-tin type crystal potential and usually have no adjustable parameters, and empirical calculations such as EPM and adjusted OPW calculations, which include a reasonable number of adjustable parameters to fit theoretical band structures to appropriately interpreted experimental data. In these latter approaches one can assume that Koopmans' corrections are incorporated in the adjustable parameters. The EPM calculations of Cohen and Bergstrasser[45] on a number of binary semiconductors has shown the success of this approach as far as levels within a few eV around the gap are concerned. The shortcomings of local pseudopotential calculations in describing the energies of deeper lying valence bands are well-known. A recent attempt, however, by

Chelikowsky, Chadi, and Cohen[35] to fit the total valence band spectra of several semiconductors with an effective electron mass as an additional free parameter was very successful, as the energies in Tables IX, X, XIV, XVI, and XVIII show.

The first-principles calculations show in general surprisingly good agreement with experiment. The self consistent calculations (SCOPW) of Stukel et al.[39,41] are clearly an improvement over the OPW calculations, especially when the Kohn-Sham exchange approximation is used (see Tables X and XVI).

The KKR calculations of Eckelt,[42] in general predict the overall bandwidth and the position of the lowest band very well for ZnS, ZnSe, and ZnTe. The best overall agreement with experiment, however, was obtained in most cases by a relativistic OPW approach, with $X_{\alpha\beta}$ exchange.[38,44] This approach appeared to possess the ability to bring the features near the top of the band down and also to move the "Peak III" features down toward their experimental positions. It will be very interesting to see what a self-consistent version of this "ROPW, $X_{\alpha\beta}$" approach can do.

Not included in Tables IX through XII are the results of the $\vec{k} \cdot \vec{p}$ method applied to the calculation of the band structures of GaP, GaAs, GaSb, and InP by Pollak et al.[34] and Higginbotham et al.[40] because only the positions of L_3 and X_5 can be deduced from their work.

Rather than discussing every symmetry point, we shall concentrate on the important gap $X_3 - X_1$ between Peak II and Peak III. This gap is closely related to the ionic character of the compound. Our results are compared with theory and UPS results in Table XX.

The XPS and UPS results are in quite good agreement where comparison is possible and the systematic discrepancy appears to arise mostly from different methods of data reduction. Turning to the theoretical work, the KKR II-VI results disagree erratically with experiment, from 0.8 eV low in ZnTe to 2.0 eV high in ZnS. A similar scatter is found in the OPW results ranging from -1.4 eV in GaSb to +1.5 eV in InP. The results from self-consistent OPW calculations are too few to assess any improvement in going from a non-self-consistent to a self-consistent theory. The three parameter scheme that leads to the adjusted OPW calculations contains two parameters[32] which adjust the cation and anion core levels respectively, so as to improve the band structure in terms of optical transitions. This adjustment leads, via the orthogonality condition, to an increase in the gap $X_3 - X_1$ comparable to the antisymmetric part in the pseudopotential in the EPM scheme. An inspection of Table XX reveals, however, that this adjustment in all cases but GaP overemphasizes the $X_3 - X_1$ separation. This suggests, that XPS and UPS data should be considered in such adjustments. Finally, the relativistic OPW results are on the whole in quite good agreement with experiment. It will be interesting to learn how self-consistent ROPW results will compare.

A detailed interpretation of these and other $X_1 - X_3$ gaps in terms of ionicity will be given elsewhere. The general trend--an increase from III-V to II-VI compounds--is clear in Table XX.

The gross features of the valence-band XPS spectra of the wurtzite-structure compounds CdS, CdSe, and ZnO are similar to those of the semiconductors with the zincblende structure. This is not surprising, because the immediate surroundings of each atom are almost identical in the two structures.

Two peaks at the top of the valence bands correspond to Peaks I and II respectively. Peak III, which can in the more ionic II-VI compound be identified with the anion s-level, is shifted in ZnO to 20.7 eV binding energy. The very Lorentzian-like lineshape indicates considerable lifetime broadening in this level. The true width of the corresponding band is probably appreciably smaller. Peak III is presumably masked by the Cd d-levels in CdS and CdSe. This determines its binding energy in these compounds as lying between 8 and 12 eV. The mean positions of peak I, 1.8 eV in CdS and 1.9 eV in CdSe, is in good agreement with the results of earlier UV work of Shay and Spicer.[1]

Additional fine structure in peak I cannot easily be identified with energies of the uppermost valence bands at particular symmetry points because no theoretical densities of states are available and the correlation of symmetry points in the fcc Brillouin zone with those in the extended hexagonal zone[45] is limited to a few cases. We must therefore limit the comparison of our results with calculations to the position of Γ_3, a point which corresponds to L_1 in the fcc lattice and marks the bottom of peak II (see Table XXI). The top of the valence band is again the zero of energy. It falls in CdS and CdSe with considerable certainty at the center of the Brillouin zone at the nearly degenerate (except for crystal field splittings) points Γ_6 and Γ_1. The top of the valence-band in ZnO differs from all other valence bands in showing a region of small but non-zero density of states, which extends 1.4 eV beyond the steep onset of Peak I (Fig. 10). This unique feature is an indication that the top of the valence band in ZnO does not coincide with the triple degenerate point $\Gamma_{6,1}$, but rather with the energy maximum of a presumably nondegenerate band somewhere in the Brillouin zone. It is interesting to note that a similar result has been obtained in APW calculations of the band-structure of

cubic ZnS by U. Rössler and M. Lietz,[47] in which the top of the valence band is determined by the highest band along Λ. This would correspond to a point near A for the hexagonal lattice. It is most likely that an interpretation of the valence band top along similar lines in ZnO would bear on the discussion of optical measurements[50] in this compound.

Inspection of Table XXI shows that the overall width of the upper two valence peaks (I and II) is underestimated in all theoretical approaches. It should however be noted, that the self-consistent OPW calculation of Euwema et al.[48,49] finds the lowest peak III in CdS between -10.7 and -11.5 eV, in good agreement with our experimental limits of -10 ± 2 eV. Not included in the discussion of our spectra are the effects of spin-orbit splitting on the densities of states. These effects are no greater than about 0.5 eV at certain symmetry-points in Peak I for the heaviest compounds and are not clearly resolvable in our spectra. An identification of the splitting $I_1 - I_1'$ in GaAs and ZnTe is not possible.

SUMMARY AND CONCLUSIONS

We have presented the total valence-band XPS spectra of 14 semiconductors from which the binding energies of common features are extracted empirically and tabulated. The results are also interpreted to yield experimental energies of bands at select symmetry points in the Brillouin zone and then compared with available theoretical band structures. It is shown that band-structure calculations in combination with XPS spectra provide a powerful approach to establishing the total valence band structure of semiconductors.

ACKNOWLEDGMENTS

Gifts of single crystals are gratefully acknowledged from D. Reynolds, Y. Petroff, Y. P. Shen, G. A. Somorjai, and R. Dalven. We thank J. Chelikowsky and M. L. Cohen for the valuable exchange of information and F. Hermann, D. E. Eastman, M. Cardona, and D. W. Langer and their coworkers for providing us with their results prior to publication. One of us (L.L.) greatly appreciates a grant from the Max-Kade Foundation.

FOOTNOTES AND REFERENCES

*Work performed under the auspices of the U. S. Atomic Energy Commission.

†Present Address: IBM Watson Research Center, Yorktown Heights, New York.

1. J. L. Shay and W. E. Spicer, Phys. Rev. 161, 799 (1967).

2. M. Cardona and D. L. Greenaway, Phys. Rev. 131, 98 (1963).

3. D. E. Eastman and W. D. Grobman, Phys. Rev. Letters 28, 1327 (1972); these authors point out that the spectrum taken with 40 eV photon energy still shows final state effects. It is however obvious that the UV-photoelectron spectra resemble the XPS spectrum more closely with increasing photon energy.

4. R. G. Cavell, S. P. Kowalczyk, L. Ley, R. A. Pollak, B. Mills, D. A. Shirley, and W. Perry, Phys. Rev. B, June (1973), in press.

5. K. Siegbahn, D. Hammond, H. Fellner-Feldegg, and E. F. Barnett, Science 176, 245 (1972).

6. R. A. Pollak, S. Kowalczyk, L. Ley, and D. A. Shirley, Phys. Rev. Letters 29, 274 (1972).

7. This value was obtained as the mean of many measurements in this Laboratory.

8. R. H. Bube, Photoconductivity of Solids (John Wiley, New York, 1960).

9. A comprehensive report on plasmons in XPS spectra is in preparation by the present authors.

10. W. Gudat, E. E. Koch, P. Y. Yu, M. Cardona, and C. M. Penchina, Phys. Stat. Sol. (b) 52, 505 (1972).

11. T. Lane, C. J. Veseley, and D. W. Langer, Phys. Rev. B, to be published.

12. C. J. Veseley and D. W. Langer, Phys. Rev. B4, 451 (1971).

13. M. Cardona, C. M. Penchina, E. E. Koch, and P. Y. Yu, Phys. Stat. Sol. (b) 53, 327 (1972).

14. J. L. Shay and W. E. Spicer, Phys. Rev. 169, 650 (1968).

15. C. J. Veseley, R. L. Hengehold, and D. W. Langer, Phys. Rev. 5B, 2296 (1972).

16. R. A. Powell, W. E. Spicer, and J. C. McMenamin, Phys. Rev. Letters 27, 97 (1971).

17. D. E. Eastman, W. D. Grobman, and J. Freeouf, to be published; D. E. Eastman, J. Freeouf, and M. Erbudak, Congres du Centenaire de la Societe Francaise de Physique, Vittel, France, May 28 - June 2, 1973 (unpublished).

18. M. Cardona, C. M. Penchina, N. Shevchik, and J. Tejeda, Sol. St. Comm. 11, 1655 (1972).

19. L. F. Wagner and W. E. Spicer, Phys. Rev. Letters 28, 1381 (1972).

20. D. E. Eastman and W. D. Grobman, Phys. Rev. Letters 28, 1378 (1972).

21. R. T. Poole, P. C. Kemeny, J. Liesegang, J. G. Jenkin, and R. C. G. Leckey, private communication.

22. C. E. Moore, Atomic Energy Levels (U. S. Dept. of Commerce, NBS Circular No. 467, 1958).

23. F. R. McFeely, S. P. Kowalczyk, L. Ley, R. A. Pollak, and D. A. Shirley, Phys. Rev. B, in press.

24. L. Ley, R. A. Pollak, S. P. Kowalczyk, and D. A. Shirley, Phys. Letters 41A, 429 (1972).

25. In preparation by present authors.

26. Carl J. Ballhausen, Introduction to Ligand Field Theory (McGraw-Hill, New York, 1962), p. 119; cited after W. Moffitt, G. L. Goodman, M. Fred, and B. Weinstock, Mol. Phys. 2, 109 (1959).

27. L. Ley, S. P. Kowalczyk, R. A. Pollak, and D. A. Shirley, Phys. Rev. Letters 28, 1088 (1972).

28. C. S. Fadley and D. A. Shirley, Journal of Research, NBS 74A, 543 (1970).

29. W. C. Price, A. W. Potts, and D. G. Streets, in Electron Spectroscopy, ed. by D. A. Shirley (North-Holland, Amsterdam, 1972).

30. U. Gelius, in Electron Spectroscopy, ed. by D. A. Shirley (North-Holland, Amsterdam, 1972).

31. W. E. Spicer, Phys. Rev. 154, 385 (1967).

32. F. Hermann, R. L. Kortum, I. B. Ortenburger, and J. P. van Dyke, Electronic Structure and Optical Spectrum of Semiconductors, ARL Report No. 69-0080, May 1969.

33. T. S. Koopmans, Physica 1, 104 (1934).

34. J. Chelikowsky, D. J. Chadi, and M. L. Cohen, to be published.

35. F. Hermann, R. L. Kortum, C. D. Kuglin, and J. P. van Dyke, in Methods of Computational Physics, ed. by B. Alder, S. Fernbach, and M. Roten (Academic Press, New York, 1968), p. 193. This is an OPW calculation, adjusted with three parameters to optical data.

36. Ref. 35, but a first-principles OPW calculation.

37. I. B. Ortenburger and W. E. Rudge, IBM Research Laboratory Report RJ-1041 (1972). Relativistic OPW with $X_{\alpha\beta}$ exchange.

38. D. J. Stukel, T. C. Collins, and R. N. Euwema, Electronic Density of States, NBS Special Publication 323, 1971, p. 93.

39. F. H. Pollak, C. W. Higginbotham, and M. Cardona, Proceedings of the Int. Conf. on the Physics of Semiconductors, Kyoto, 1966, J. Phys. Soc. (Japan) 21, Supplement, 20 (1966).

40. C. W. Higginbotham, F. H. Pollak, and M. Cardona, Proceedings of the Ninth International Conf. on Semiconductors, Moscow, 1968, ed. by S. M. Ryvkin (Nauka Publishing House, Leningrad, 1968), p. 57.

41. D. J. Stukel, R. N. Euwema, T. C. Collins, F. Hermann, and R. L. Kortum, Phys. Rev. 179, 740 (1969).

42. P. Eckelt, Phys. Stat. Sol. 23, 307 (1967).

43. U. Rössler and M. Lietz, Phys. Stat. Sol. 17, 597 (1966).

44. J. P. van Dyke and F. Hermann, private communication.

45. T. K. Bergstrasser and M. L. Cohen, Phys. Rev. 164, 1069 (1967).

46. U. Rössler, Phys. Rev. 184, 733 (1969).

47. U. Rössler and M. Lietz, Phys. Stat. Sol. 17, 597 (1966).

48. T. C. Collins, R. N. Euwema, and J. S. De Witt, Proceedings of the International Conf. on Physics of Semiconductors, Kyoto, 1966, J. Phys. Soc. (Japan) 21, Supplement, 15 (1966).

49. R. N. Euwema, T. C. Collins, D. G. Shankland, and J. S. De Witt, Phys. Rev. 162, 710 (1967).

50. J. O. Dimmock, in Proceedings of the International Conference on II-VI Semiconducting Compounds, Providence, 1967, ed. by G. Thomas (W. A. Benjamin, Inc., New York, 1967), p. 588 and references therein.

Table I. Structures of materials studied in this work.

Group	Compound	Structure[a]	lattice constant a, in Å[b]
III-V	GaP	z	5.448
"	GaAs	z	5.6534
"	GaSb	z	6.095
"	InP	z	5.869
"	InAs	z	6.058
"	InSb	z	6.478
II-VI	ZnO	w(1.60)	3.249
"	ZnS	z	5.406
"	ZnSe	z	5.667
"	ZnTe	z	6.1026
"	CdS	w(1.62)	4.136
"	CdSe	w(1.63)	4.299
"	CdTe	z	6.481
"	HgTe	z	6.453

[a] z = zincblende, w = wurtzite (c/a in parenthesis).

[b] From "Powder Diffraction File", published by Joint Committee on Powder Diffraction Standards, Swarthmore, Pennsylvania, 19081 (1972).

Table II. Surface contaminations of semiconductor samples as measured *in situ*

	monolayers of oxygen[a]	$\frac{OK}{CK}$
GaP	< 0.1	--
GaAs	0.2	1
GaSb	0.2	large
InP	0.2	1.9
InAs	< 0.1	--
InSb	0.6	0.8
CdS	< 0.1	--
CdSe	< 0.1	--
CdTe	0.4	0.4
ZnS	< 0.1	--
ZnSe	0.5	0
ZnTe	0.6	0.2
HgTe	0.4	0.6

[a]Deduced from comparison with oxygen signal from ZnO; estimated error 100%.

Table III. Relative positions of the gold-evaporated Fermi level and the top of the semiconductor valence bands, in eV.

Compound	$E_F - E_{VB}$	Gap Energy[a]	Approximate location of E_F[b]
CdS	1.27	2.58	C
CdSe	1.88	1.84	T
CdTe	0.47	1.40	C
GaP	0.15	2.26	B
GaAs	0.0	1.40	B
InAs	0.3	0.35	T
ZnO	1.63	3.3	C
ZnS	1.08	3.6	C
ZnSe	1.13	2.80	C
ZnTe	0.17	1.19	B
InSb	0.12	0.18	C

[a] These are averages of a large number of values in the literature.

[b] T = top, C = center, and B = bottom of gap.

Table IV. Binding energies of outermost d-levels of cation for different compounds. All values in eV. Errors in the last place are given parenthetically.

Compound	E_B^F	E_B^V	Method[a]	Reference
CdS	10.91(9)		XPS, Au	this work
	11.35(20)		XPS, C	12
		9.64(15)	XPS	this work
		9.2 (2)	UPS	14
		10.0 (4)	UPS	15
CdSe	11.92(9)		XPS, Au	this work
	11.48(20)		XPS, C	12
		10.04(15)	XPS	this work
		9.9 (2)	UPS	14
		10.7 (4)	UPS	15
CdTe	10.96(9)		XPS, Au	this work
	11.09(48)		XPS, C	12
		10.49(15)	XPS	this work
		10.3 (2)	UPS	1
		10.5 (4)	UPS	15
		10.2 (2)	UPS	17
ZnO	10.44(9)		XPS, Au	this work
	10.34(20)		XPS, C	12
		8.81(15)	XPS	this work
		8.5 (4)	UPS	15
		7.5 (2)	UPS	16
ZnS	10.11(9)		XPS, Au	this work
	10.27(20)		XPS, C	12
		9.03(15)	XPS	this work
ZnSe	10.33(9)		XPS, Au	this work
	10.39(20)		XPS, C	12
		9.20(15)	XPS	this work
		8.9 (4)	UPS	15

(continued)

Table IV. (continued)

Compound	E_B^F	E_B^V	Method[a]	Reference
ZnTe	10.01(9)		XPS, Au	this work
	9.93(38)		XPS, C	12
		9.84(15)	XPS	this work
		9.1 (4)	UPS	15
GaP	18.70(15)		XPS, Au	this work
	18.9 (2)		XPS, Au	11
	19.2 (2)		XPS, --	10
		18.55(10)	XPS	this work
GaAs	18.82(9)		XPS, Au	this work
	19.0 (2)		XPS, Au	11
	19.3 (2)		XPS, --	10
		18.82(15)	XPS	this work
		18.7 (1)	UPS	18
GaSb	20.1 (2)		XPS, --	10
		19.00(15)	XPS	this work
InP	17.7 (2)		XPS, --	10
		16.80(15)	XPS	this work
InAs	17.40(9)		XPS, Au	this work
	17.5 (2)		XPS, Au	11
	17.2 (2)		XPS, --	10
		17.09(15)	XPS	this work
InSb	17.41(9)		XPS, Au	this work
	17.3 (2)		XPS, Au	11
	16.8 (2)		XPS, --	10
		17.29(15)	XPS	this work
		17.49(10)	UPS	17
		17.31(10)	UPS	18
HgTe	$d_{5/2}$ $d_{3/2}$			
	7.53(20) 9.44(20)		XPS, C	12
		$d_{5/2}$ $d_{3/2}$		
		7.87(15) 9.64(15)	XPS	this work
		7.6 (4) 9.5 (4)	UPS	15

[a] Au = referred to $E_B^F Au(4f_{7/2})$ = 84.00(1) eV. C = referred to E_B^F(C 1s) = 283.8 eV.

Table V. Binding energies of the outermost anion d-level for different compounds; all energies are in eV. Errors in the last place are given parenthetically.

Compound	E_B^F $d_{5/2}$	E_B^F $d_{3/2}$	E_B^V $d_{5/2}$	E_B^V $d_{3/2}$	Method[a]	Reference
ZnTe	40.40(12)	41.87(12)			XPS, Au	this work
	39.97(29)	41.47(24)			XPS, C	12
			40.23(15)	41.70(15)	XPS	this work
CdTe	39.97(8)	41.41(8)			XPS, Au	this work
	39.92(31)	41.42(25)			XPS, C	12
			39.50(15)	40.94(15)	XPS	this work
HgTe	39.68(20)	41.12(20)			XPS, C	12
			39.89(15)	41.33(15)	XPS	this work
PbTe[c]	39.49(7)	40.95(7)			XPS, Au	this work
	39.6 (3)	40.95(30)			XPS, Au[b]	13
			39.49(15)	40.95(15)	XPS	this work
GaSb	31.45(20)	32.6 (2)			XPS,	10
			31.58(15)	32.79(15)	XPS	this work
InSb	31.57(9)	32.79(12)			XPS, Au	this work
	31.44(20)	32.8 (20)			XPS, Au	11
	31.05(20)	32.20(20)			XPS, --	10
			31.45(15)	32.67(15)	XPS	this work
			31.27(10)	32.52(10)	UPS	17
ZnSe	54.63(9)				XPS, Au	this work
			53.50(15)		XPS	this work
PbSe[c]	53.35(30)	54.2 (30)			XPS, Au[b]	13
	53.7(3)					
			53.50(10)		XPS	this work

(continued)

Table V. (continued)

Compound	E_B^F $d_{5/2}$	$d_{3/2}$	E_B^V $d_{5/2}$	$d_{3/2}$	Method[a]	Reference
GaAs	40.76(9)				XPS, Au	this work
	41.1 (2)				XPS, Au	11
	40.8 (2)				XPS, --	10
			40.76(15)		XPS	this work
InAs	40.61(9)				XPS, Au	this work
	40.9 (2)				XPS, Au	11
	40.7 (2)				XPS, --	10
			40.30(15)		XPS	this work

[a]See footnote a on Table IV.

[b]The values are corrected to the Au reference by increasing the binding energies by 0.7 eV as suggested in Ref. 13.

[c]These values are included for comparison.

Table VI. Spin-orbit splittings (in eV).

Sample	Shell	Splitting	Reference
Zn II	Zn3d	0.337	22
Zn metal	"	0.54(2)[a]	21
Cd II	Cd4d	0.669	22
Cd metal	"	0.95(3)	21
Cd metal	"	0.99(5)	6
CdTe	"	0.70(5)	17
CdTe	"	0.83(20)	12
CdS	"	0.76(12)	12
CdSe	"	0.87(16)	12
In III	In4d	0.849	22
In metal	"	0.90(1)	6
In metal	"	0.88(15)	17
In metal	"	0.86(3)	21
InSb	"	0.83(3)	18
InSb	"	0.85(5)	17
InSb	"	0.84(8)	this work
InP	"	0.84(8)	this work
Sb V	Sb4d	1.239	22
Sb metal	"	1.25(4)	6
GaSb	"	1.21(4)	this work
InSb	"	1.22(4)	this work
InSb	"	1.15(10)	18
InSb	"	1.25(5)	17
Te VII	Te4d	1.409	22
Te metal	"	1.51(1)	6
ZnTe	"	1.47(2)	this work
CdTe	"	1.44(2)	this work
HgTe	"	1.44(2)	this work
PbTe	"	1.46(2)	this work
PbTe	"	1.35(10)	18

(continued)

Table VI. (continued)

Sample	Shell	Splitting	Reference
Hg II	Hg5d	1.864	22
liquid Hg	"	1.83(9)	this work
HgTe	"	1.77(2)	this work
HgTe	"	1.91(10)	12
HgSe	"	1.81(10)	12
HgS	"	1.79(10)	12
Pb IV	Pb4d	2.643	22
Pb metal	"	2.62(2)	24
Pb metal	"	2.66(9)	21
PbS	"	2.58(2)	23
PbSe	"	2.61(2)	23
PbTe	"	2.61(2)	23

[a]Error in last place.

Table VII. Binding energies of characteristic valence-band features from top of valence bands (in eV).[a]

Material	H_{IT}	I_2	I_1	I_1'	S_1	H_{IB}	E_I	H_{IIT}	P_{II}	H_{IIB}	E_{II}	E_{III}	H_{IIIT}	P_{III}	H_{IIIB}	B
GaP	0.7	1.7	2.4	--	3.5	4.0	--	5.4	6.5	7.0	7.4	8.2	9.1	10.3	12.2	13.4
GaAs	1.0	1.8	2.4	2.9	3.8	--	--	--	6.6	7.5	8.1	9.0	10.0	11.4	13.3	14.4
GaSb	0.8	1.7	2.1	--	3.4	3.7	4.4	5.5	6.4	7.1	7.4	8.6	9.2	10.0	11.1	11.9
InP	0.7	--	1.8	--	2.7	3.6	--	--	5.4	6.2	6.9	7.8	8.6	9.7	10.8	11.6
InAs	0.6	1.7	2.1	--	3.0	3.5	--	--	5.8	6.3	6.9	8.5	9.4	10.5	11.6	12.6
InSb	1.0	2.0	2.5	--	3.2	3.5	4.2	--	5.9	6.5	7.2	8.4	8.9	10.0	11.1	12.0
ZnO	2.1	--	2.9	--	≈3.8	--	--	--	5.9	6.6	7.0	≈18	19.8	20.7	23.1	24.8
ZnS	0.8	2.0	2.6	--	3.2	4.0	--	--	4.9	5.9	6.4	11.4	11.8	12.4	13.3	13.8
ZnSe	0.8	1.6	1.9	--	2.6	3.5	--	--	5.2	5.8	6.0	11.6	12.1	13.1	14.6	15.8
ZnTe	0.7	1.2	1.7	2.2	2.8	3.4	--	--	5.1	5.8	6.3	11.3	11.5	11.9	12.7	13.4
CdS	0.8	1.3	1.6	--	2.1	3.1	--	--	4.1	4.8	5.5	--	--	--	--	--
CdSe	0.8	1.5	1.9	--	--	--	--	--	4.3	5.1	5.5	--	--	--	--	--
CdTe	0.6	1.5	1.8	--	2.5	2.9	(3.6)	--	4.5	5.2	5.6	--	--	--	--	--
HgTe	0.7	1.5	2.1	--	--	3.3	--	--	5.3	6.0	6.4	--	--	--	--	--

[a]See Fig. 15 and text for definition of points. Accuracy is ±0.1 eV.

LBL-1688

Table VIII. Comparison of characteristic features in valence band spectra from XPS (this work) and UPS (Ref. 17) in eV.[a]

Material	I_1		S_1		P_{II}		P_{III}		B	
	XPS	UPS	XPS	UPS	XPS	UPS	XPS	UPS	XPS	UPS
GaP	2.4	1.6	3.5	3.6	6.5	6.5	10.3	10.2	13.4	12.3
GaAs	2.4	1.7	3.8	3.6	6.6	6.4	11.4	11.2	14.4	13.6
InSb	2.5	1.9	3.2	3.4	5.9	6.0	10.0	9.9	12.0	11.7
ZnSe	1.9	1.3	2.6	2.7	5.2	4.9	13.1	13.7	15.8	--
CdTe	1.7	1.5	2.5	2.5	4.5	4.4	--	--	--	--
Ge	2.6	2.6	3.8	3.8	7.4	7.7	10.5	10.6	13.2	12.8

[a]Relative to top of valence bands. Quoted values were obtained graphically from both sets of spectra.

Table IX. Valence-band energies in GaP (in eV with respect to the top of the valence-band).

Method	L_3	X_5	W_2	Σ_1^{min}	W_1	$X_3(L_1)$	X_1	L_1	Γ_1	Ref.
XPS	1.2(3)	2.7(2)	3.6(2)	4.0(2)	6.5(2)	6.9(2)	9.6(3)	10.6(3)	13.2(4)	this work
UPS	0.8	--	--	4.1	--	6.9	9.7	--	11.8	17
EPM(adj)	1.0	2.5	3.7	4.1	6.6	6.9	10.9	11.7	13.6	34
OPW(adj)	0.9	2.3	--	--	--	6.1	9.2	10.0	11.8	35
OPW[a]	0.9	2.3	--	--	--	6.1	9.4	10.1	11.9	36
ROPW,$X_{\alpha\beta}$	0.9	2.2	--	--	--	6.1	9.5	10.3	12.0	37

[a]Kohn-Sham exchange.

Table X. Valence-band energies in GaAs (in eV with respect to the top of the valence-band).

Method	L_3	X_5	W_2	Σ_1^{min}	W_1	$X_3(L_1)$	X_1	L_1	Γ_1	Ref.
XPS	1.4(3)	2.5(3)	4.0(2)	4.4(2)	6.6(1)	7.1(2)	10.7(3)	12.0(5)	13.8(4)	this work
UPS	0.8	--	--	4.1	--	6.9	10.0	--	12.9	17
EPM(adj)	0.9	2.5	3.5	3.9	6.6	6.8	11.4	--	13.8	34
OPW(adj)	0.9	2.3	--	--	--	5.6	10.7	11.1	12.4	35
OPW[a]	1.0	2.3	--	--	--	6.3	9.7	10.4	12.0	36
ROPW,$X_{\alpha\beta}$	1.1	2.4	--	--		6.4	10.2	10.9	12.4	37
SCOPW[a]	1.0	2.5	3.4	4.0	6.2	6.6	9.2	10.1	11.9	38
SCOPW[b]	1.0	2.3	3.0	3.3	6.0	6.3	9.5	10.2	11.8	38

[a]Kohn-Sham exchange.

[b]Slater exchange.

Table XI. Valence-band energies in GaSb (in eV with respect to the top of the valence-band).

Method	L_3	X_5	W_2	Σ_1^{min}	W_1	$X_3(L_1)$	X_1	L_1	Γ_1	Ref.
XPS	1.3(2)	2.7(2)	2.6(2)	3.8(2)	6.4(1)	6.9(3)	9.4(2)	10.3(3)	11.6(3)	this work
OPW(adj)	0.9	2.3	--	--	--	5.5	9.8	9.9	11.1	35
OPW[a]	1.1	2.4	--	--	--	6.3	7.9	9.0	10.7	36
ROPW,$X_{\alpha\beta}$	1.2	2.5	--	--	--	6.9	8.9	9.7	11.3	37

[a]Kohn-Sham exchange.

Table XII. Valence-band energies in InP (in eV with respect to the top of the valence-band).

Method	L_3	X_5	W_2	Σ_1^{min}	W_1	$X_3(L_1)$	X_1	L_1	Γ_1	Ref.
XPS	1.0(3)	2.0(2)	2.5(2)	3.2(2)	5.4(2)	5.9(2)	8.9(3)	10.0(3)	11.0(4)	this work
OPW(adj)	0.6	1.7	--	--	--	4.6	9.7	10.1	11.1	32
OPW[a]	0.6	1.7	--	--	--	4.5	9.0	9.4	10.6	32
ROPW,$X_{\alpha\beta}$	0.7	1.6	--	--	--	4.6	9.2	9.7	10.8	37

[a]Kohn-Sham exchange.

Table XIII. Valence-band energies in InAs (in eV with respect to the top of the valence-band).

Method	L_3	X_5	W_2	Σ_1^{min}	W_1	$X_3(L_1)$	X_1	L_1	Γ_1	Ref.
XPS	0.9(3)	2.4(3)	2.7(3)	3.3(2)	5.8(2)	6.3(2)	9.8(3)	10.6(3)	12.3(4)	this work
OPW(adj)	0.6	1.7	--	--	--	4.7	10.3	10.6	11.5	32
OPW[a]	0.7	1.8	--	--	--	4.7	9.4	9.8	10.8	32
ROPW,$X_{\alpha\beta}$	0.8	1.9	--	--	--	5.1	10.0	10.4	11.4	37

[a]Kohn-Sham exchange.

Table XIV. Valence-band energies in InSb (in eV with respect to the top of the valence-band).

Method	L_3	X_5	W_2	Σ_1^{min}	W_1	$X_3(L_1)$	X_1	L_1	Γ_1	Ref.
XPS	1.4(3)	2.4(4)	3.1(2)	3.4(2)	5.9(2)	6.4(2)	9.5(2)	10.5(3)	11.7(3)	this work
UPS	1.05	--	--	3.65	--	6.5	9.0	--	11.2	17
EPM(adj)	1.2	2.1	2.8	3.2	5.7	6.2	9.5	10.1	11.3	34
OPW(adj)	0.7	1.8	--	--	--	4.7	9.0	9.3	10.2	32
OPW[a]	0.8	1.9	--	--	--	5.0	7.7	8.3	9.6	32
ROPW,$X_{\alpha\beta}$	1.1	2.1	--	--	--	5.7	8.8	9.3	10.5	37

[a]Kohn-Sham exchange.

Table XV. Valence-band energies of ZnS (in eV with respect to the top of the valence-band).

Method	L_3	X_5	W_2	Σ_1^{min}	W_1	$X_3(L_1)$	X_1	L_1	Γ_1	Ref.
XPS	1.4(4)	2.5(3)	3.0(2)	3.4(3)	4.9(2)	5.5(2)	12.0(3)	12.4(3)	13.5(4)	this work
OPW(adj)	0.3	1.1	--	--	--	3.5	--	--	--	41
OPW[a]	0.4	1.2	--	--	--	3.5	--	--	--	41
ROPW,$X_{\alpha\beta}$	0.5	1.3	--	--	--	3.8	11.2	11.5	12.2	44
SCOPW	0.6	1.6	2.0	2.1	3.7	4.2	10.0	10.6	11.7	41
KKR	0.6	1.4	--	2.1	--	3.3	11.9	12.1	12.6	42
APW	0.9	1.7	--	--	--	3.4	13.4	13.4	14.0	43

[a]Slater exchange.

Table XVI. Valence-band energies in ZnSe (in eV with respect to the top of the valence-band).

Method	L_3	X_5	W_2	Σ_1^{min}	W_1	$X_3(L_1)$	X_1	L_1	Γ_1	Ref.
XPS	1.3(3)	2.1(3)	2.6(2)	3.4(2)	5.2(2)	5.6(3)	12.5(4)	13.1(3)	15.2(6)	this work
UPS	0.7	--	--	3.4	--	5.3	--	--	--	17
EPM(adj)	0.9	2.1	3.3	3.8	5.3	5.9	14.2	14.5	15.8	34
OPW(adj)	0.4	1.4	--	--	--	3.7	--	--	--	35
OPW[b]	0.4	1.3	--	--	--	3.8	--	--	--	36
ROPW,$X_{\alpha\beta}$	0.7	1.6	--	--	--	4.2	11.6	11.9	12.6	44
SCOPW[a]	0.7	2.0	2.7	3.1	4.5	4.7	10.4	10.8	11.8	38
SCOPW[b]	0.7	1.6	2.3	4.5	4.2	4.4	10.5	10.9	11.8	38
KKR	0.6	1.3	--	2.2		3.6	12.0	12.2	12.6	42

[a] Kohn-Sham exchange.

[b] Slater exchange.

Table XVII. Valence-band energies of ZnTe (in eV with respect to the top of the valence-band).

Method	L_3	X_5	W_2	Σ_1^{min}	W_1	$X_3(L_1)$	X_1	L_1	Γ_1	Ref.
XPS	1.1(3)	2.4(2)	2.7(2)	3.2(3)	5.1(2)	5.5(2)	11.6(3)	12.0(3)	13.0(4)	this work
OPW(adj)	0.5	1.4	--	--	--	3.7	--	--	--	35
OPW[a]	0.6	1.5	--	--	--	4.4	--	--	--	36
ROPW,$X_{\alpha\beta}$	1.0	2.0	--	--	--	5.0	10.2	10.6	11.5	44
KKR	0.6	1.6	--	2.8	--	4.3	9.6	9.7	10.5	42

[a]Slater exchange.

Table XVIII. Valence-band energies of CdTe (in eV with respect to the top of the valence-band).

Method	L_3	X_5	W_2	Σ_1^{min}	W_1	$X_3(L_1)$	X_1	L_1	Γ_1	Ref.
XPS	0.9(3)	1.8(2)	2.2(3)	2.7(3)	4.5(2)	5.1(2)	--	--	--	this work
UPS	0.7	--	--	2.8	--	4.7	8.8	--	--	17
EPM(adj)	1.0	1.5	2.0	2.7	4.3	4.6	10.6	--	11.8	34
OPW(adj)	0.4	1.1	--	--	--	3.0	--	--	--	35
OPW[a]	0.4	1.1	--	--	--	3.1	--	--	--	36
ROPW,$X_{\alpha\beta}$	0.8	1.6	--	--	--	3.9	10.1	10.3	10.8	44
KKR	0.6	1.4	--	2.1	--	3.5	8.7	9.2	10.3	42

[a]Slater exchange.

Table XIX. Valence-band energies of HgTe (in eV with respect to the top of the valence-band).

Method	L_3	X_5	Σ_1^{min}	W_1	$X_3(L_1)$	X_1	Γ_1	Ref.
XPS	1.2(2)	2.5(3)	3.2(3)	5.3(2)	5.7(3)	--	--	this work
ROPW, $X_{\alpha\beta}$	0.8	1.6	--	--	4.8	10.2	10.9	44

Table XX. The $X_1 - X_3$ Gap (eV)

Material	KKR[42]	OPW[38a]	OPW_{adj}[37]	SCOPW[38a]	SCOWP[38b]	ROPW[37,44]	XPS[c]	UPS[17,47]
GaP		3.3	3.1			3.4	2.7	2.8
GaAs		3.4	5.1	2.6	3.2	3.8	3.6	3.1
GaSb		1.1	4.3			2.0	2.5	
InP		4.5	5.1			4.6	3.0	
InAs		4.7	5.6			4.9	3.5	
InSb		2.7	4.3			3.1	3.1	2.5
ZnS	8.6				5.8[41]	7.4	6.5	
ZnSe	8.4			5.7	6.1	7.4	6.9	
ZnTe	5.3					5.2	6.1	
CdTe	5.2					6.2	--	4.1

[a] With Kohn-Sham exchange.

[b] With Slater exchange.

[c] This work.

Table XXI. Energy of point Γ_3 in the Brillouin zone with respect to $\Gamma_{1,6}$ for hexagonal CdS, CdSe, and ZnO (in eV).

	XPS	KKR[a]	OPW[b]	SCOPW[c]	EPM[d]
CdS	5.0 ± 0.4		3.4	3.6	2.8
CdSe	5.2 ± 0.3				2.5
ZnO[e]	5.2 ± 0.3	3.8			

[a] Ref. 46.

[b] Ref. 48.

[c] Ref. 49.

[d] Ref. 45.

[e] $\Gamma_{6,1}$ is assumed to be the zero intercept of the linear extrapolation of the maximum slope at the leading edge of Peak I.

FIGURE CAPTIONS

Fig. 1. The charging of insulators and semiconductors under x-ray bombardment as measured by XPS versus the energy of the fundamental band gap.

Fig. 2. X-ray photoelectron spectra from GaP, GaAs, and GaSb.

Fig. 3. X-ray photoelectron spectra from InP, InAs, and InSb.

Fig. 4. X-ray photoelectron spectra from ZnO, ZnS, ZnSe, and ZnTe.

Fig. 5. X-ray photoelectron spectra from CdS, CdSe, and CdTe.

Fig. 6. X-ray photoelectron spectrum from HgTe.

Fig. 7. The splitting of a d-hole-state in the presence of a tetrahedral field and spin-orbit coupling. ξ is the spin-orbit coupling constant.

Fig. 8. The corrected valence-band spectra, I'(E), of GaP, GaAs, and GaSb.

Fig. 9. The corrected valence-band spectra, I'(E), of InP, InAs, and InSb.

Fig. 10. The corrected valence-band spectrum, I'(E), of ZnO.

Fig. 11. The corrected valence-band spectra, I'(E), of ZnS, ZnSe, and ZnTe.

Fig. 12. The corrected valence-band spectra, I'(E), of CdS, CdSe, and CdTe.

Fig. 13. The corrected valence-band spectrum, I'(E), of HgTe.

Fig. 14. Generalized photoelectron spectrum for the binary semiconductors. For an explanation of the labeled features see text.

Fig. 15. Amplitudes of the radial 2s and 2p wavefunctions for carbon, R(C 2s) and R(C 2p), compared with the radial wavefunctions of free electrons χ in states corresponding to 20 eV and 1486 eV kinetic energy, respectively.

Fig. 16. Band structure, density of states $\rho(E)$, broadened density of states $\rho'(E)$, and corrected valence-band spectrum I'(E) for GaP. Band structure and $\rho(E)$ are taken from Ref. 34.

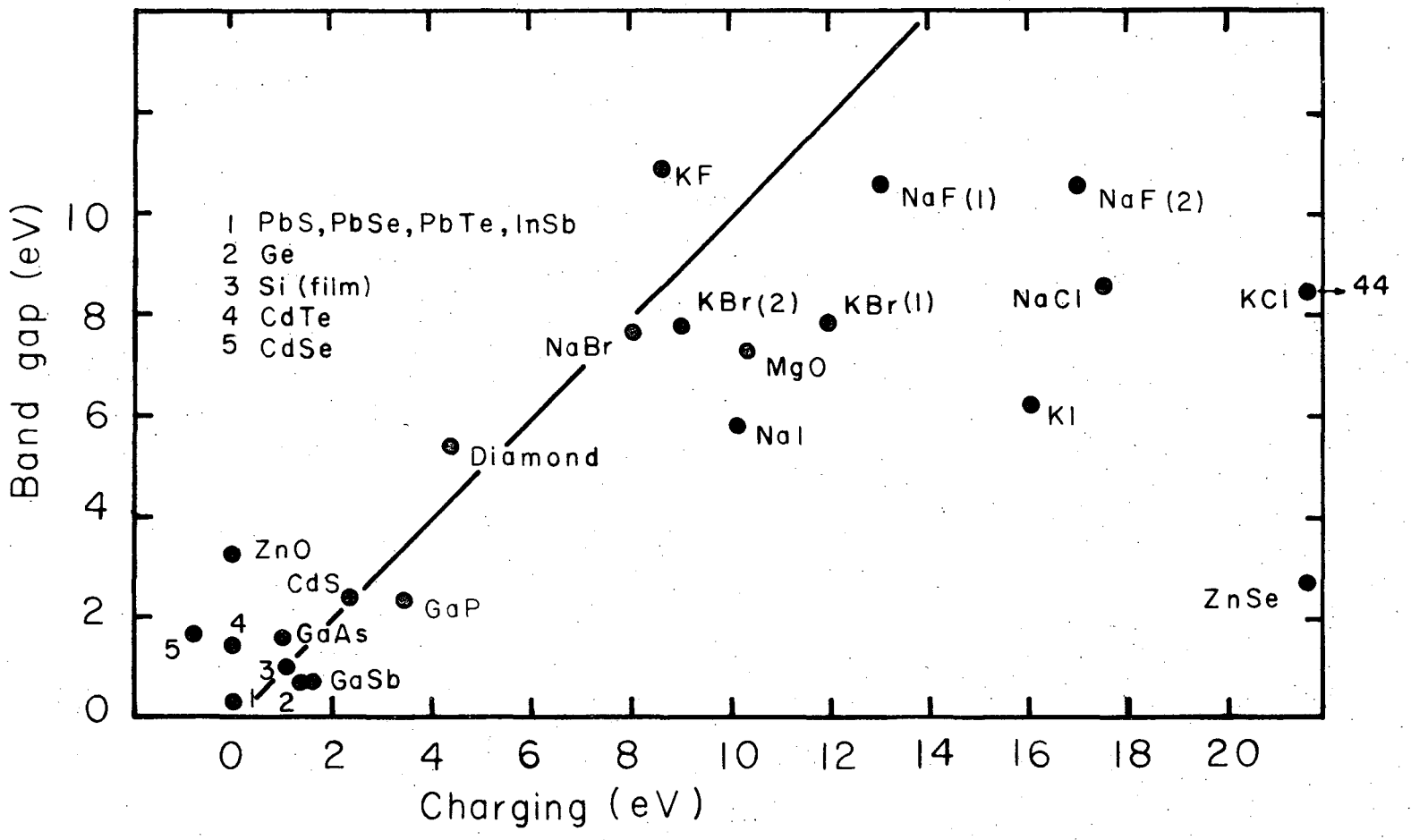

XBL 7211-7406

Fig. 1

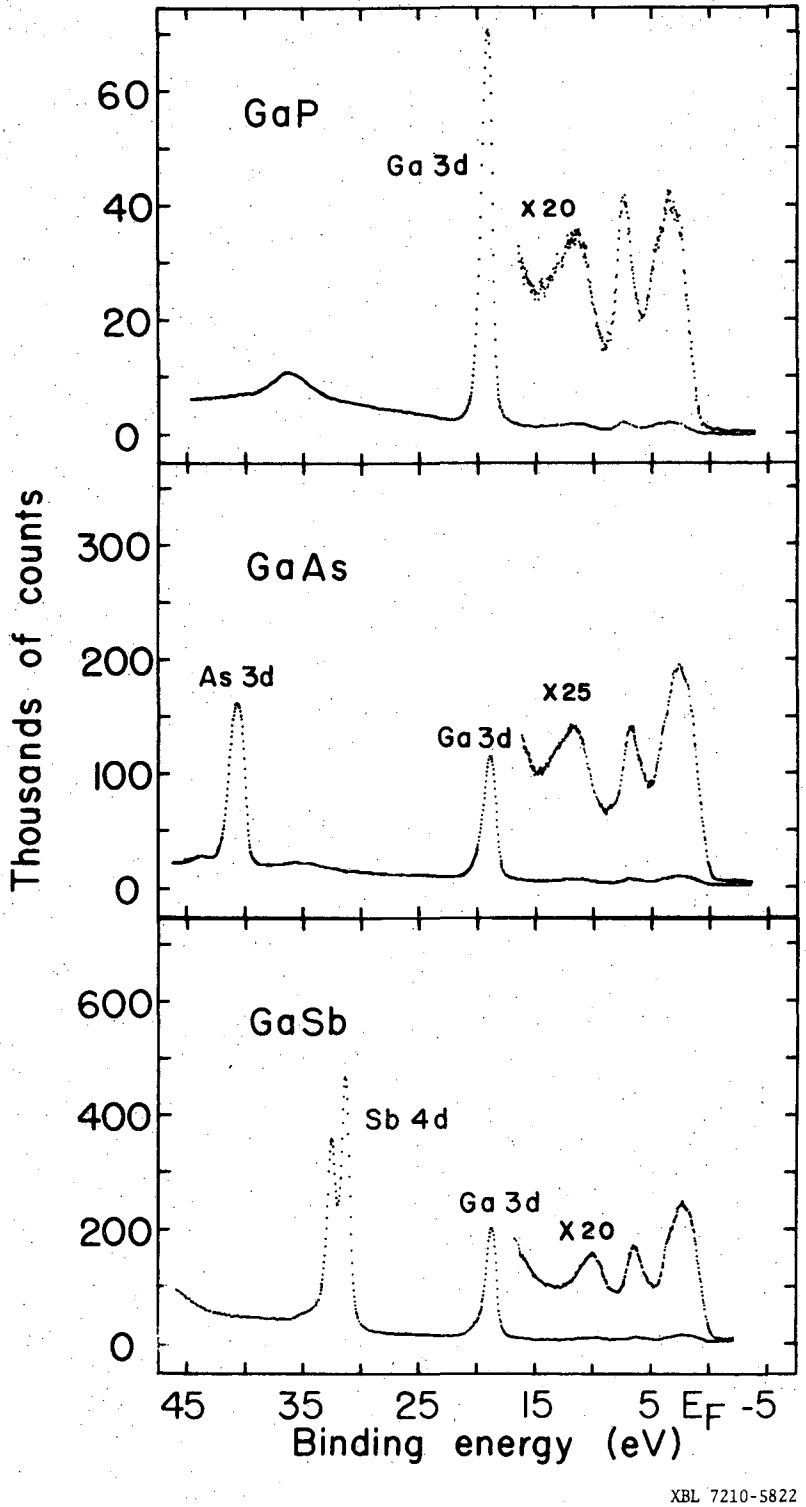
GaP
Ga 3d
X20
GaAs
As 3d
X25
Ga 3d
GaSb
Sb 4d
Ga 3d
X20
Thousands of counts
60
40
20
0
300
200
100
0
600
400
200
0
45
35
25
15
5
E_F
-5
Binding energy (eV)
XBL 7210-5822

Fig. 2

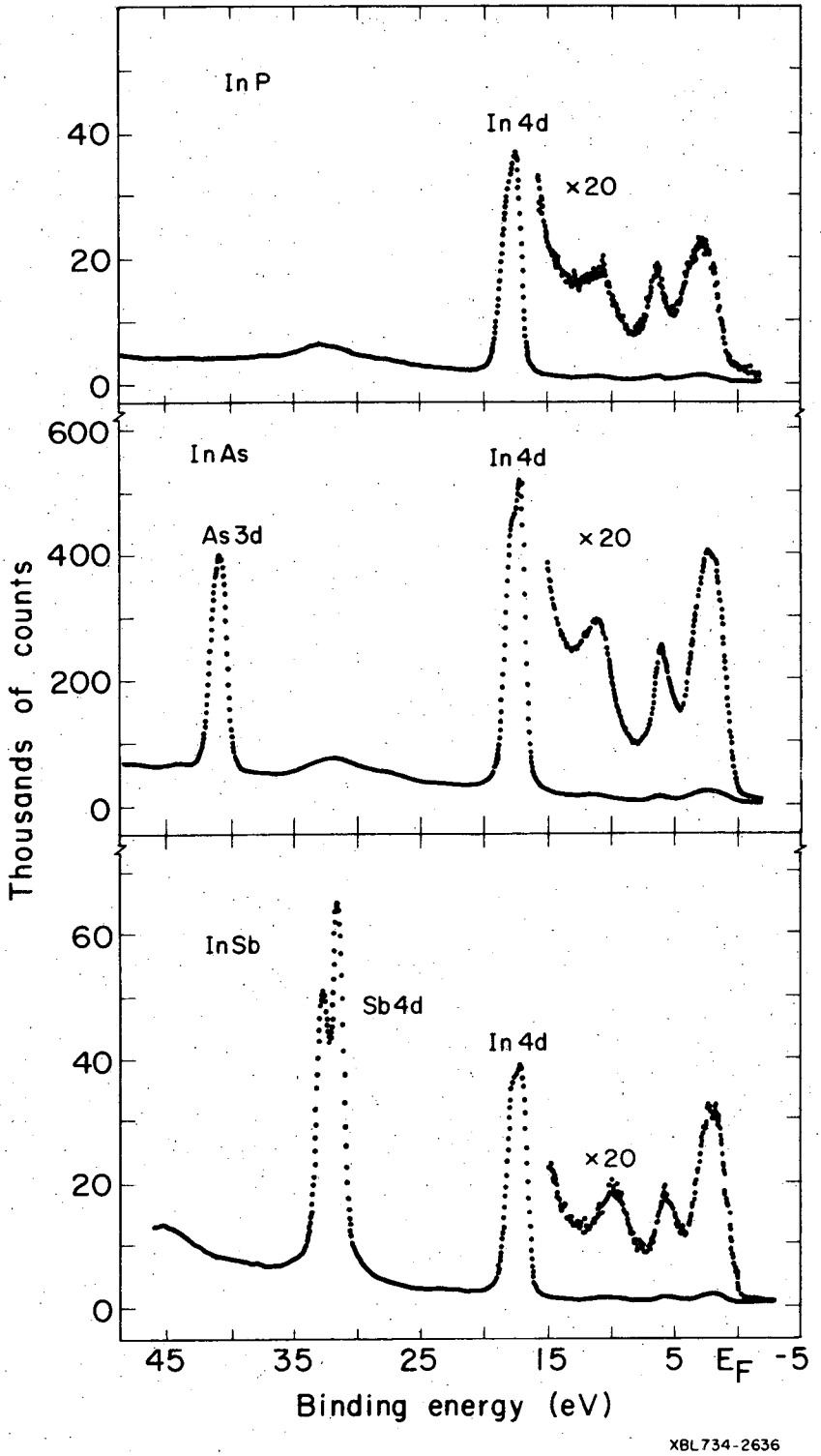
InP
In 4d
×20
40
20
0
InAs
In 4d
As 3d
×20
600
400
200
0
Thousands of counts
InSb
Sb 4d
In 4d
×20
60
40
20
0
45
35
25
15
5
E_F
-5
Binding energy (eV)
XBL734-2636

Fig. 3

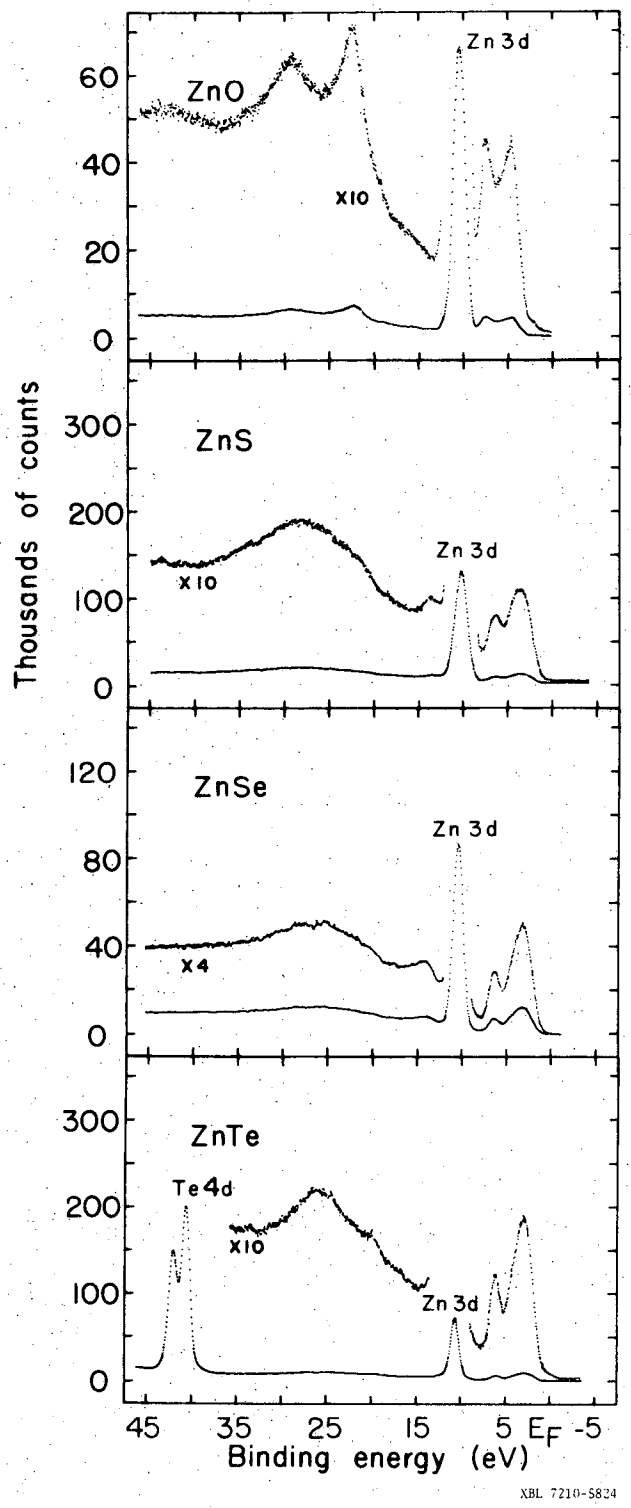
ZnO
Zn 3d
x10
ZnS
Zn 3d
x10
ZnSe
Zn 3d
x4
ZnTe
Te 4d
x10
Zn 3d
Thousands of counts
Binding energy (eV)
45
35
25
15
5
E_F
-5
XBL 7210-5824

Fig. 4

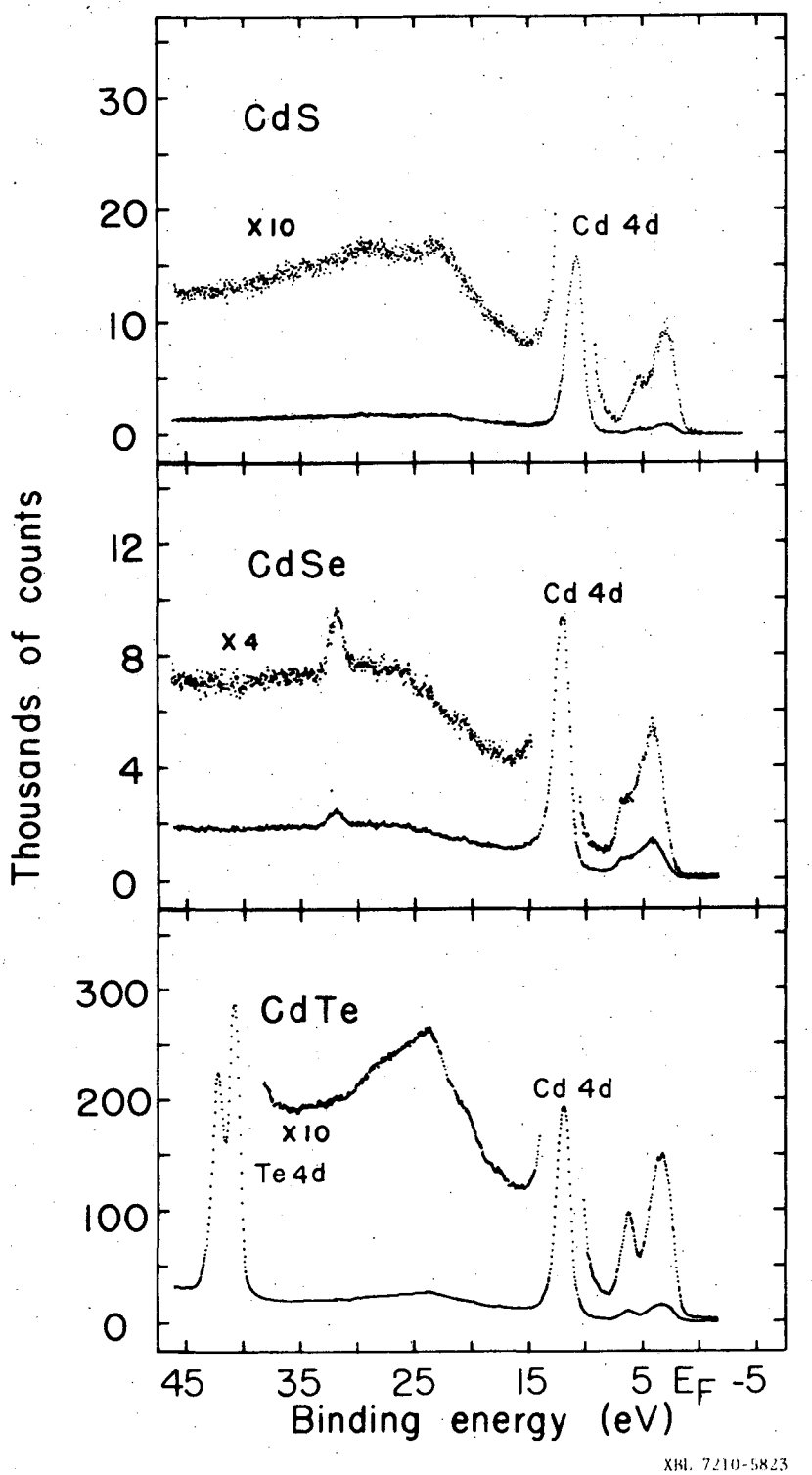
CdS
x10
Cd 4d
CdSe
x4
Cd 4d
CdTe
x10
Te 4d
Cd 4d
Thousands of counts
Binding energy (eV)
45
35
25
15
5
E_F
-5
XBL 7210-5823

Fig. 5

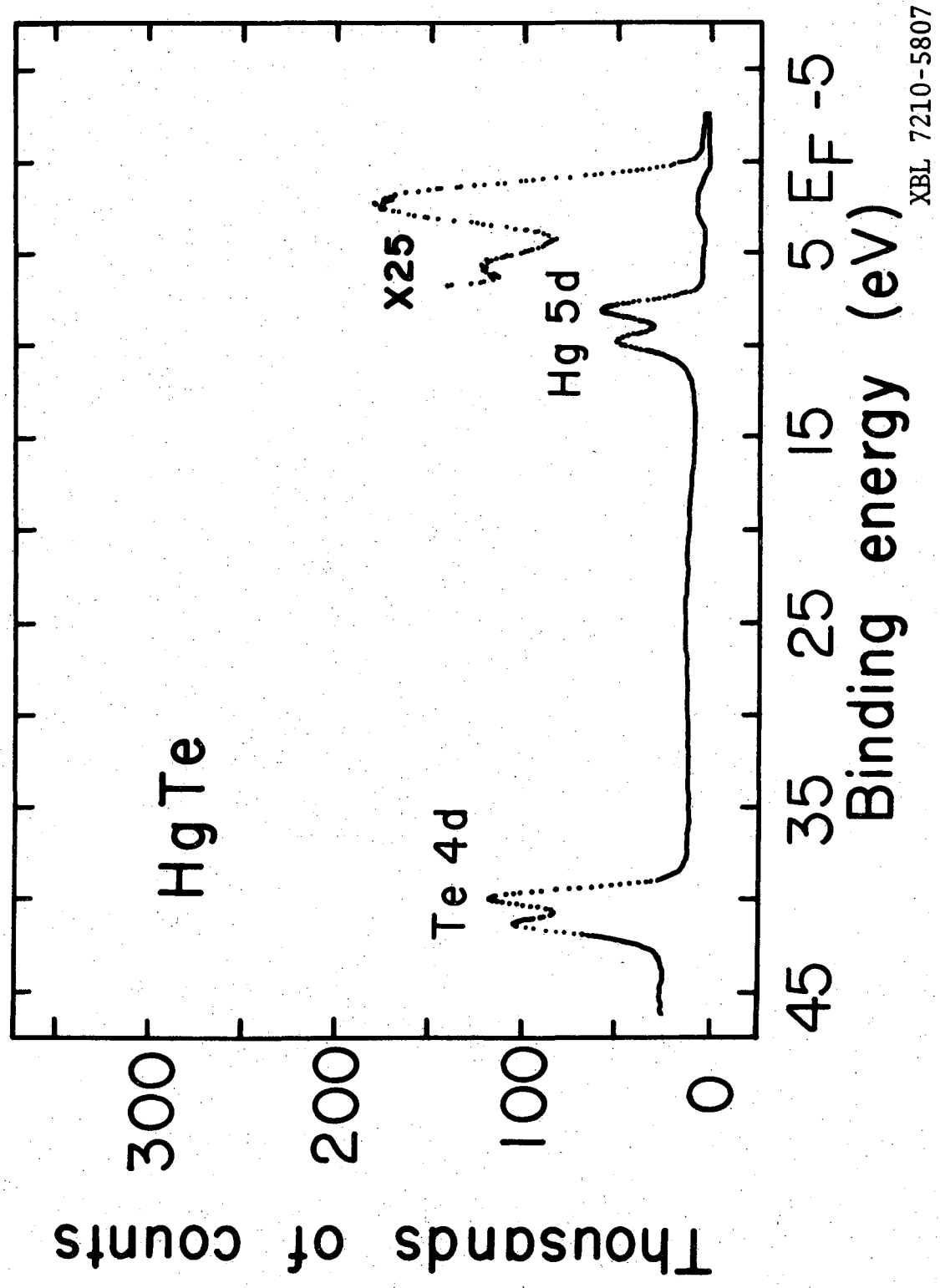
Thousands of counts
300
200
100
0
HgTe
Te 4d
Hg 5d
X25
45
35
25
15
5
E_F -5
Binding energy (eV)
XBL 7210-5807

Fig. 6

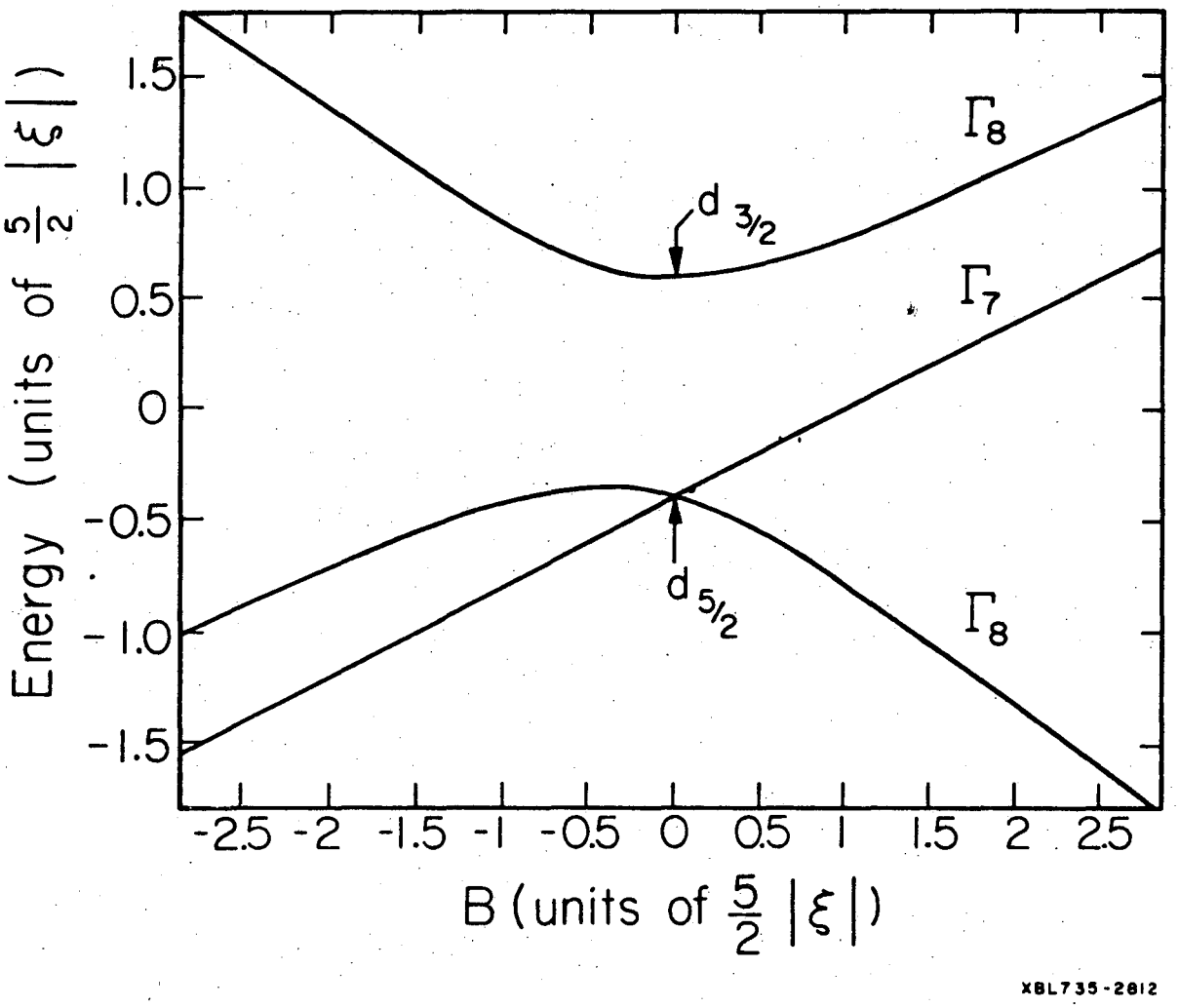
Energy (units of $\frac{5}{2}|\xi|$)
1.5
1.0
0.5
0
-0.5
-1.0
-1.5
Γ_8
$d_{3/2}$
Γ_7
$d_{5/2}$
Γ_8
-2.5 -2 -1.5 -1 -0.5 0 0.5 1 1.5 2 2.5
B (units of $\frac{5}{2}|\xi|$)
XBL735-2812

Fig. 7

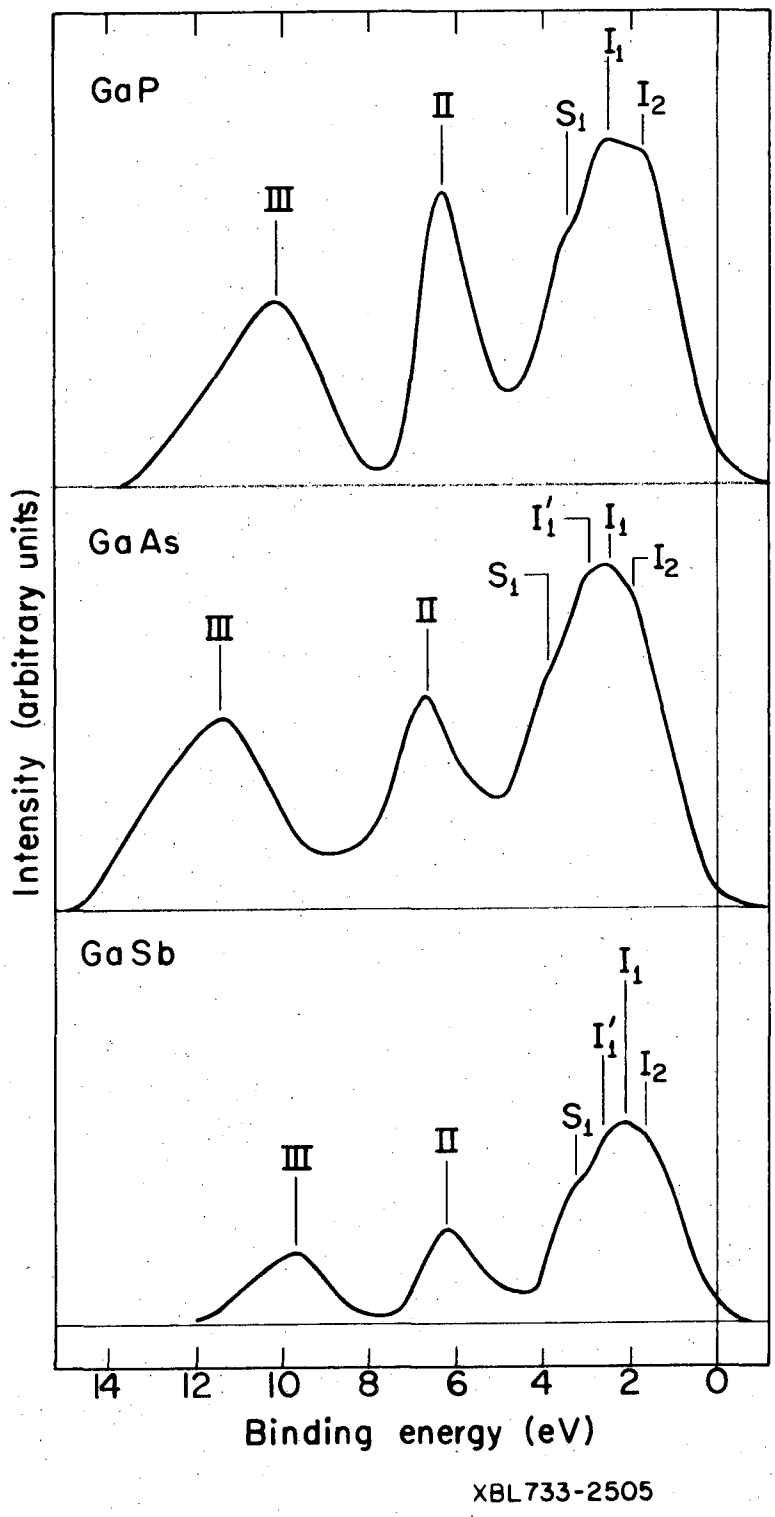
GaP
III
II
S1
I1
I2
GaAs
III
II
S1
I1'
I1
I2
GaSb
III
II
S1
I1'
I1
I2
Intensity (arbitrary units)
14
12
10
8
6
4
2
0
Binding energy (eV)
XBL733-2505

Fig. 8

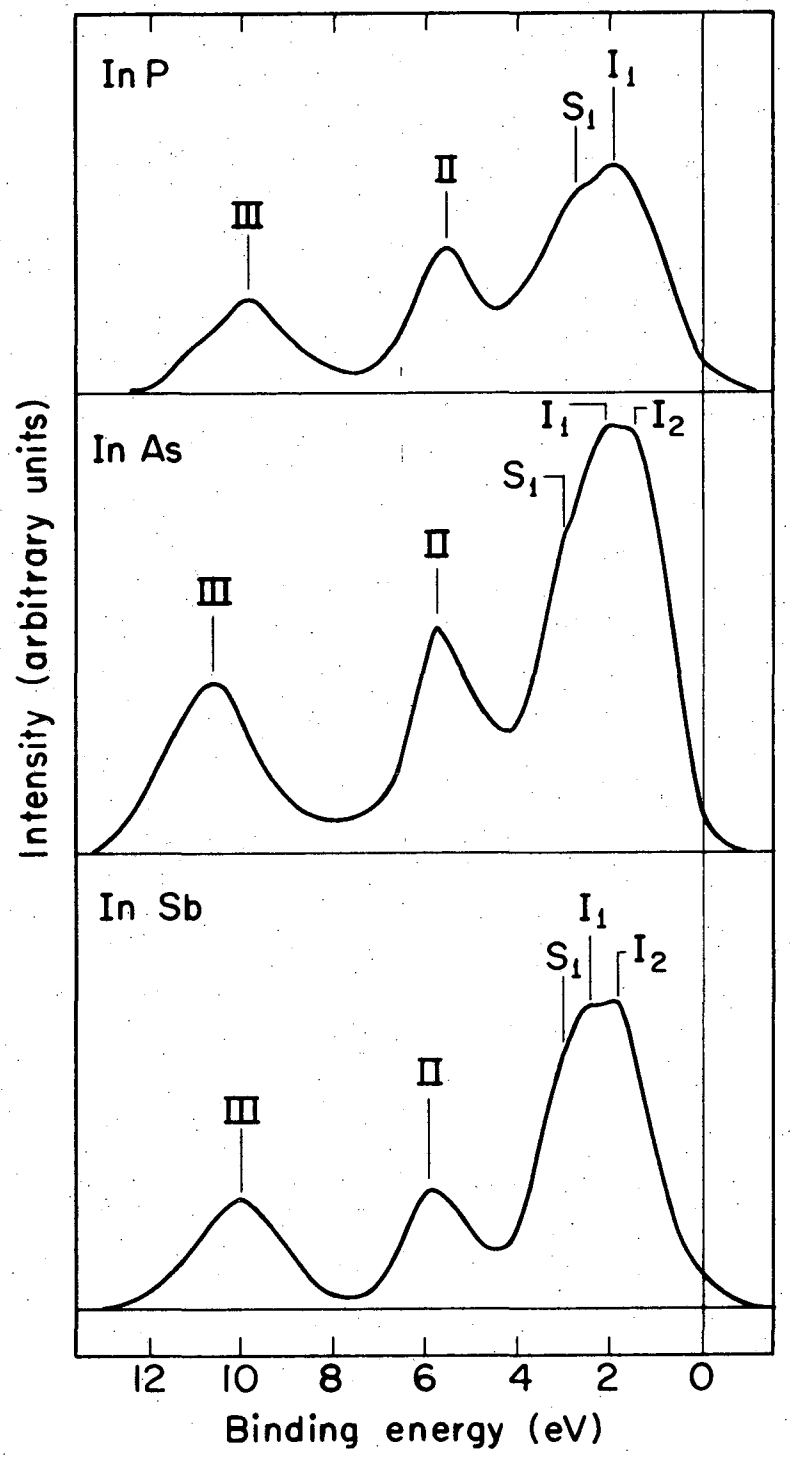
In P
I1
S1
II
III
In As
I1
I2
S1
II
III
In Sb
I1
S1
I2
II
III
Intensity (arbitrary units)
12
10
8
6
4
2
0
Binding energy (eV)
XBL733-2506

Fig. 9

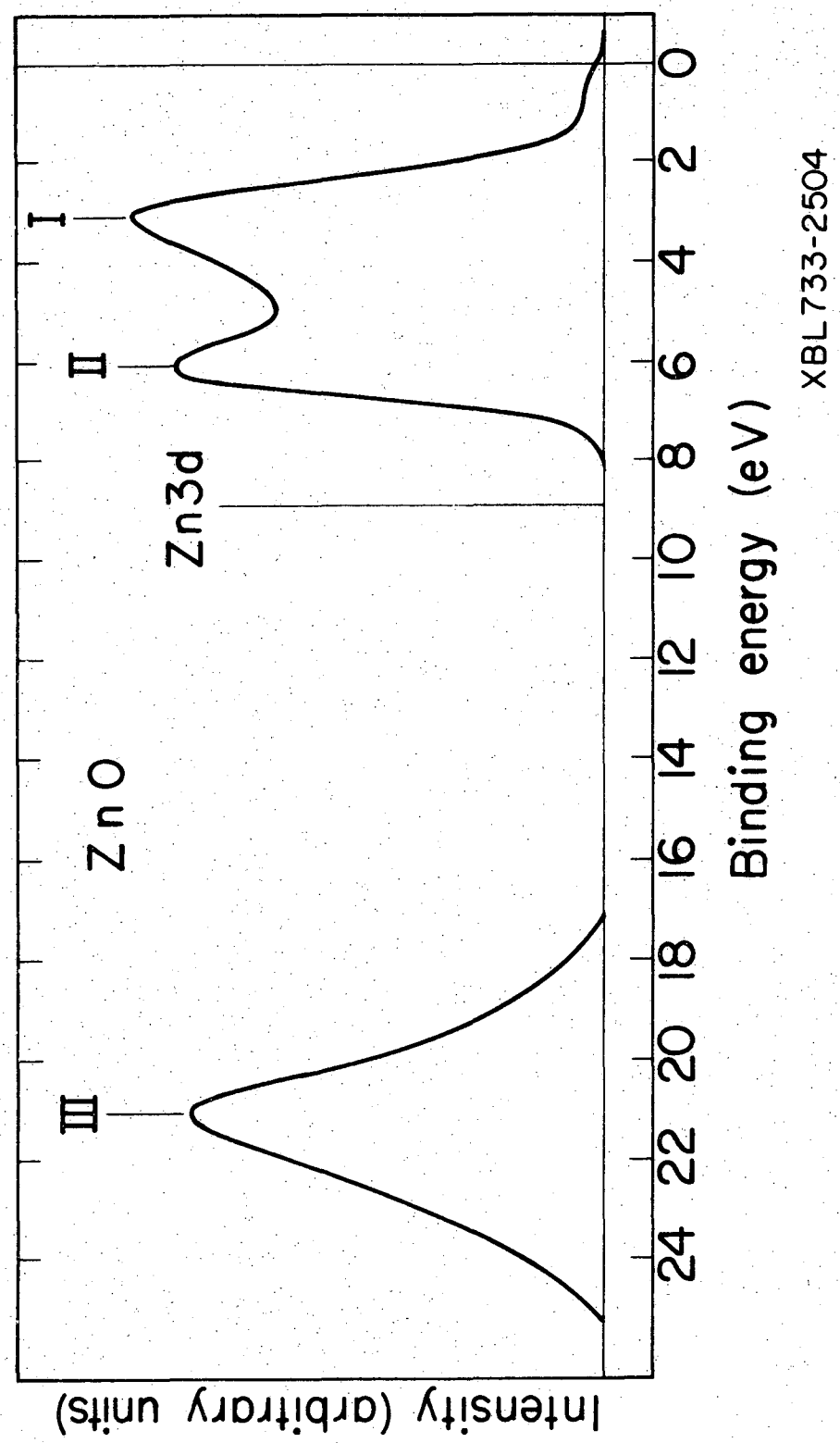
Intensity (arbitrary units)
Binding energy (eV)
0
2
4
6
8
10
12
14
16
18
20
22
24
I
II
III
Zn3d
ZnO
XBL733-2504

Fig. 10

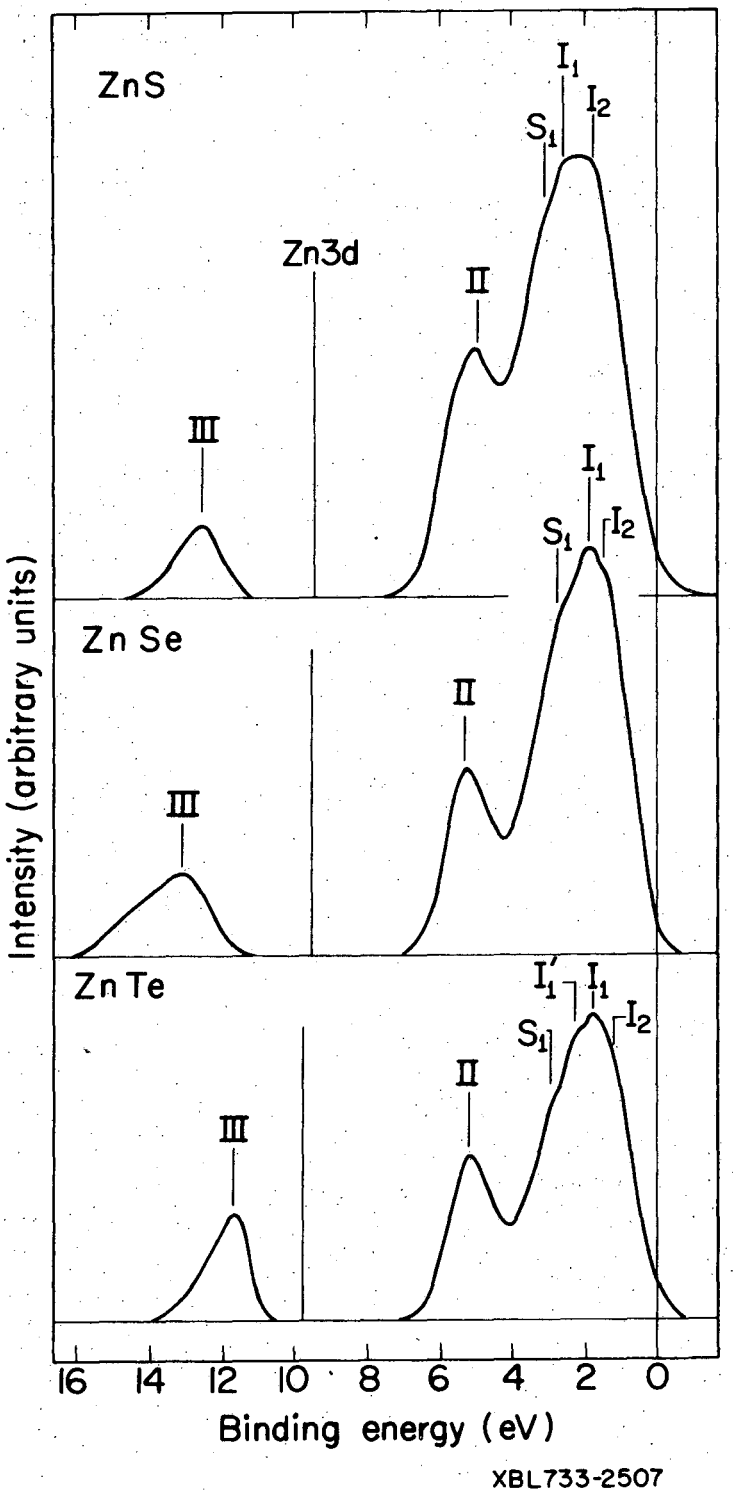
ZnS
I1
I2
S1
Zn3d
II
III
I1
S1
I2
Zn Se
II
III
I1'
I1
S1
I2
Zn Te
II
III
Intensity (arbitrary units)
16
14
12
10
8
6
4
2
0
Binding energy (eV)
XBL733-2507

Fig. 11

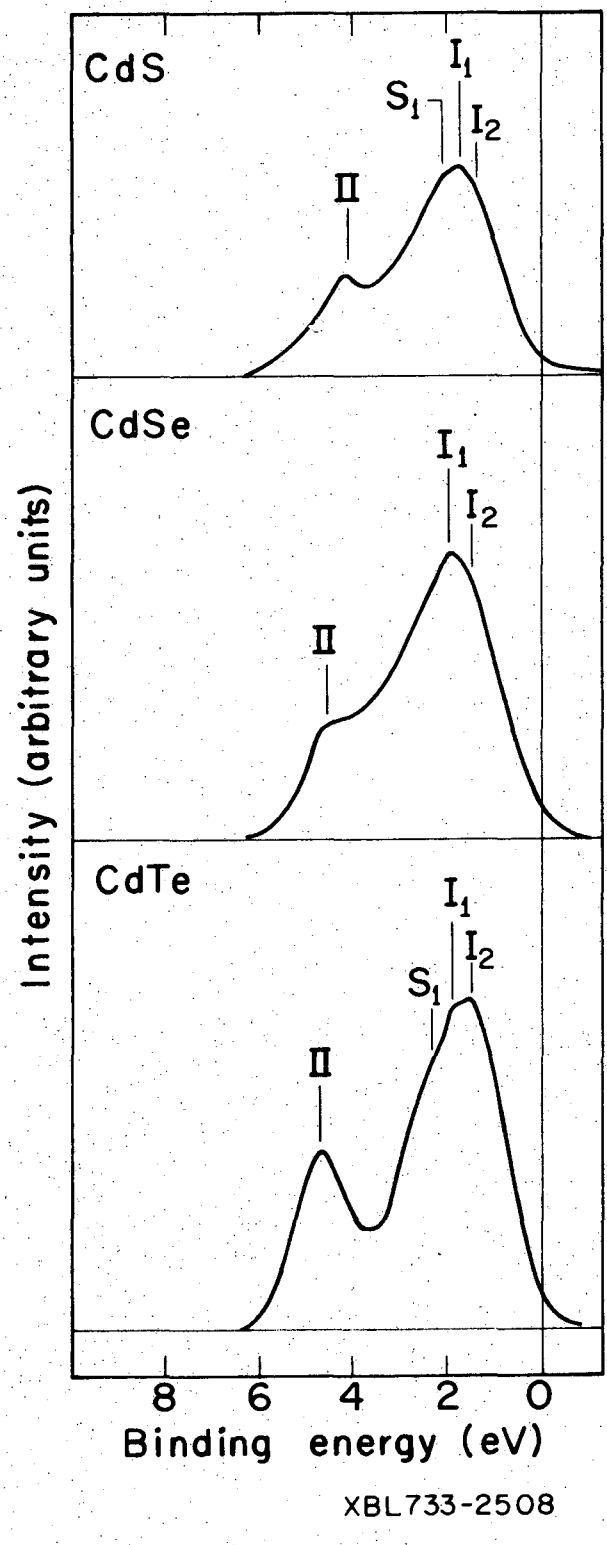
CdS
I1
S1
I2
II
CdSe
I1
I2
II
CdTe
I1
I2
S1
II
Intensity (arbitrary units)
8
6
4
2
0
Binding energy (eV)
XBL733-2508

Fig. 12

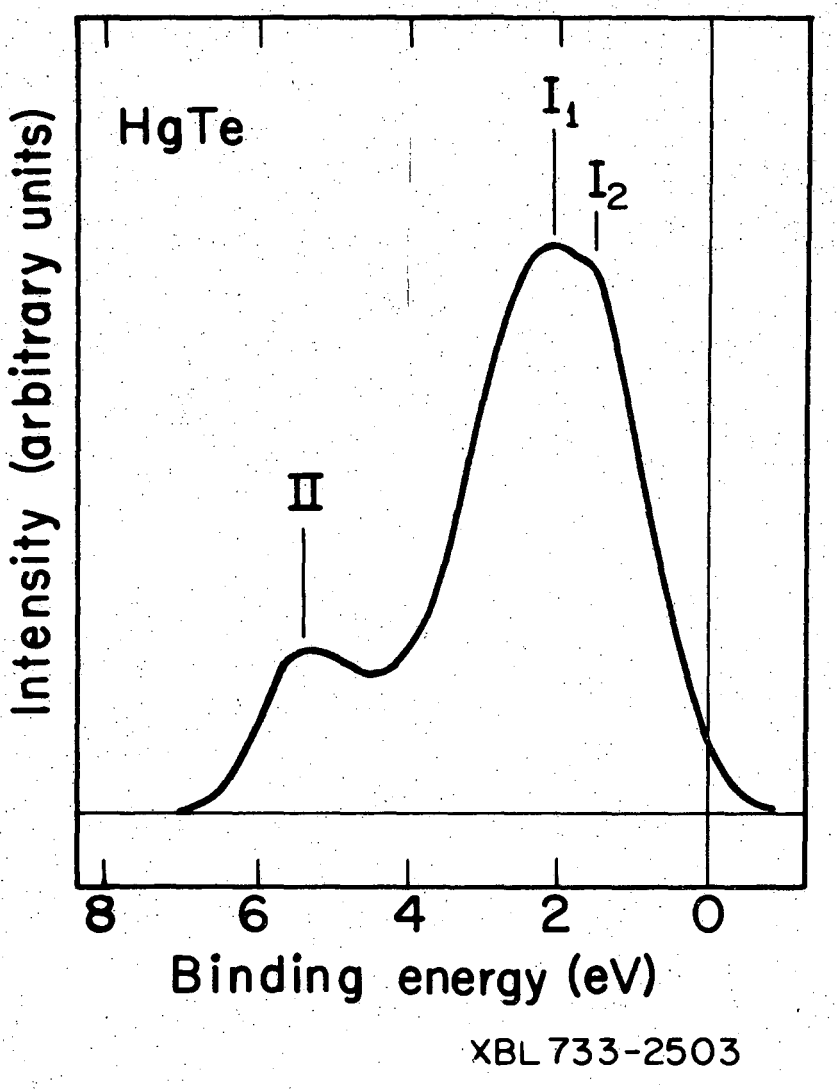
HgTe
I1
I2
II
Intensity (arbitrary units)
8
6
4
2
0
Binding energy (eV)
XBL 733-2503

Fig. 13

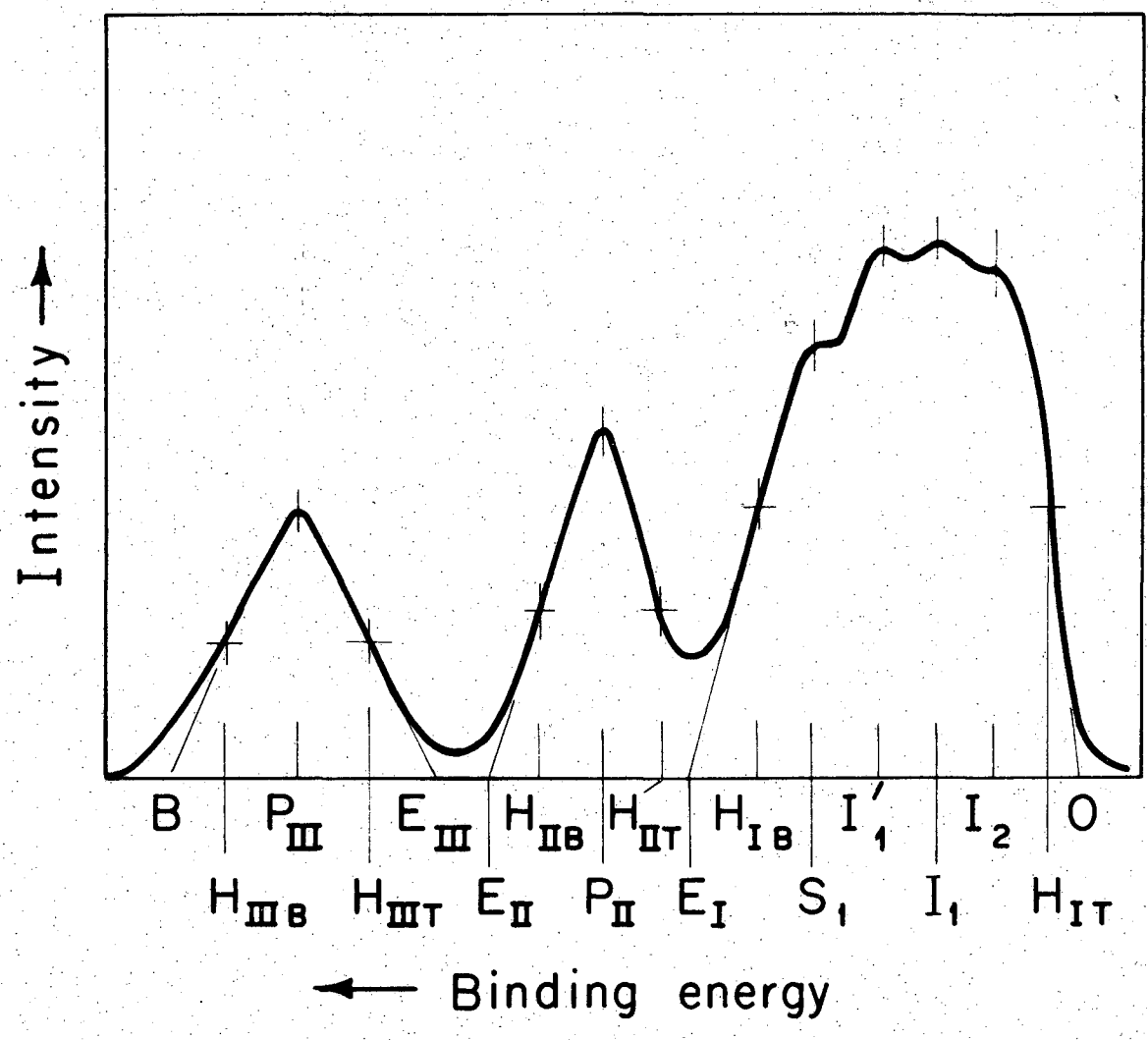

XBL735-2813

Fig. 14

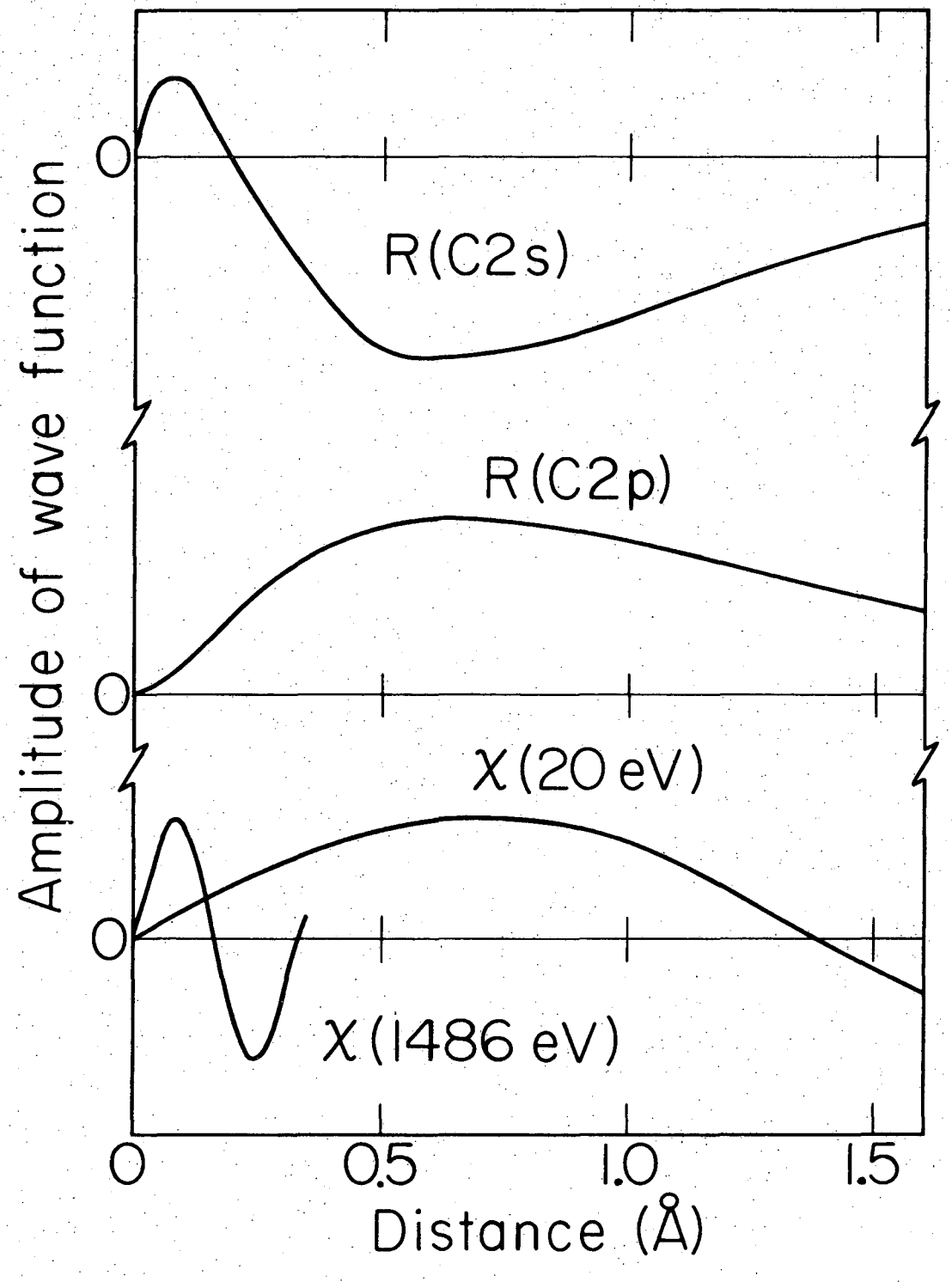

XBL7212-4883

Fig. 15

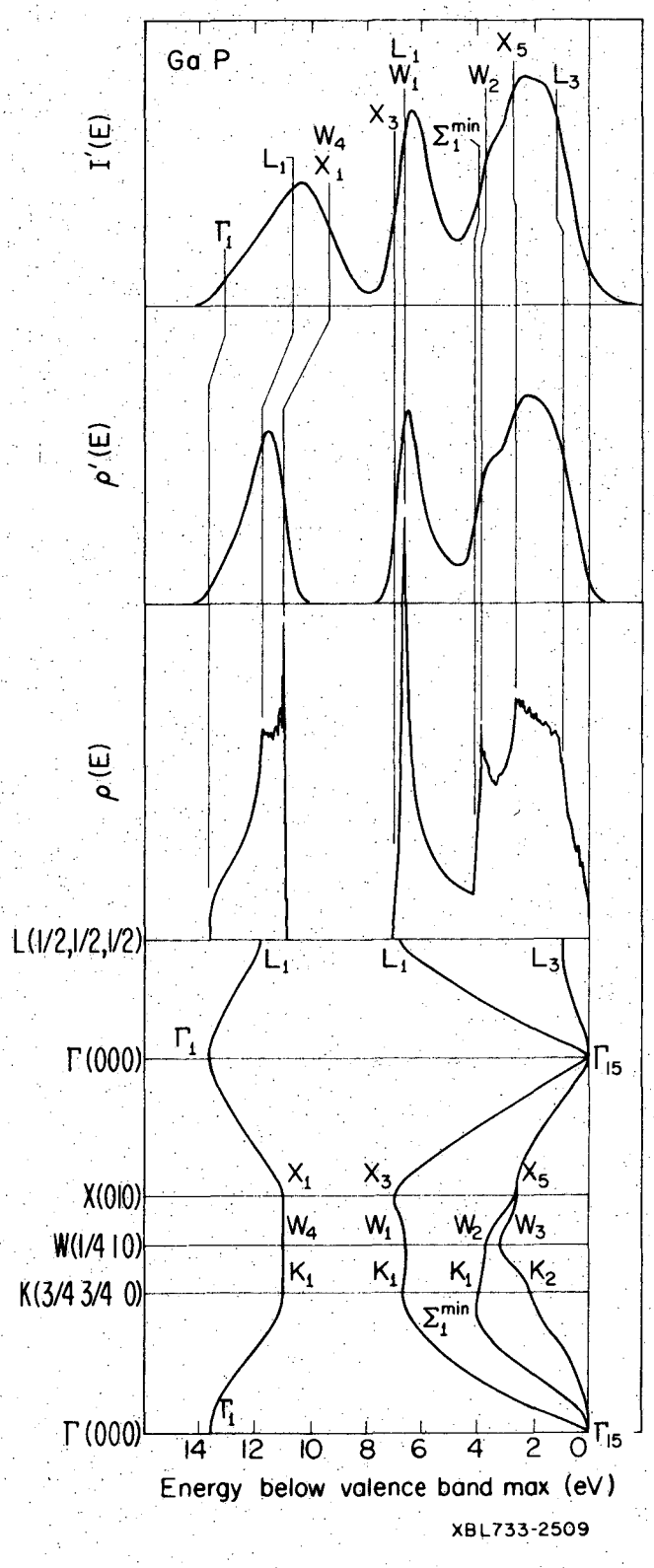
Ga P
I'(E)
ρ'(E)
ρ(E)
L(1/2,1/2,1/2)
Γ(000)
X(010)
W(1/4 1 0)
K(3/4 3/4 0)
Γ(000)
Γ1
L1
W4
X1
X3
L1
W1
Σ1min
W2
X5
L3
Γ15
K1
K2
W3
14
12
10
8
6
4
2
0
Energy below valence band max (eV)
XBL733-2509

Fig. 16

TECHNICAL INFORMATION DIVISION
LAWRENCE BERKELEY LABORATORY
UNIVERSITY OF CALIFORNIA
BERKELEY, CALIFORNIA 94720